UNIVERSITY OF MESSINA

Department of Biomedical and Dental Sciences and of Morphological and Functional Images

PhD in: TRANSLATIONAL MOLECULAR MEDICINE AND SURGERY

XXXVI Cycle

SSD: MED/30

Coordinator: Prof. Antonio Toscano

Deep learning models for the identification of retinal abnormality signs in OCT images

PhD Student:

Dr. Leandro Inferrera

Tutor:

Prof. Pasquale Aragona

ACADEMIC YEAR 2022/2023

Index

1. INTRODUCTION

1.1 AI in Clinical Practice and Applied to Ophthalmology

Radiology, dermatology, and ophthalmology are just a few of the medical specialties where AI is now used extensively. More specifically, deep learning (DL) algorithms have shown promise in detecting conditions like pulmonary tuberculosis using chest radiographs, differentiating melanomas from benign skin lesions in digital images, and detecting several diseases using fundus images or optical coherence tomography (OCT) scans. [1, 2]

In ophthalmology, AI has shown effectiveness in recognizing several retinal pathologies from fundus photographs and OCT images. [3-7] Initial studies primarily focused on posterior segment pathologies, with DL algorithms later being applied to the anterior segment as well. [7]

1.1.1 Anterior Segment

Clinical anterior segment conditions requiring imaging for patient management can be studied using AI. [7]

1.1.1.1 Cornea

The cornea is one of the structures analyzed using AI algorithms. Particularly interesting areas include:

- Keratoconus
- Refractive Surgery
- Infectious Keratitis
- Corneal Transplantation
- Pterygium

Progressive bilateral corneal ectasia, which causes myopia, abnormal astigmatism, and visual impairment, is a key characteristic of the keratoconus. The implementation of targeted therapy intended to stop or delay the progression of the pathology is made

possible by prompt detection. The first study applying AI to keratoconus dates to 1997, the results highlighted a high capacity of the AI algorithm to identify keratoconus in a test set comprising 150 video keratographies. [8] The ability to distinguish between eyes that are healthy and those that have keratoconus has improved over time, with new algorithms and classification approaches obtaining accuracy, sensitivity, and specificity levels between 92% and 97%. [7]

Additionally, artificial intelligence has found use in predicting the prognosis of patients following therapy, notably in estimating the quality of vision following surgical operations. [9] Machine learning has shown equivalent safety and predictability in the field of refractive surgery while exceeding the surgeons group in identifying patients with a higher risk of iatrogenic ectasia.[10] Identifying this category of patients during preoperative examinations is complex due to minimal alterations in corneal surface or thickness, but it is essential for predicting outcomes after any laser vision correction. [11]

Infectious keratitis can result in corneal opacities. Currently, the gold standard for detecting the microorganisms causing infectious keratitis is corneal scraping combined with microscopy, staining, and culture. However, only 33% to 80% of the time does this strategy provide favorable results. [12] In a study a diagnostic accuracy in detecting infectious keratitis of 90.7% has been achieved through a DL system, in comparison to 62.6% accuracy of clinically diagnoses. Additionally, the specificity rates for identifying bacterial and fungal keratitis from images of corneal ulcers were 100% and 76.5%, respectively. [13] Moreover artificial intelligence can assist in identifying the cause as well as reducing discrepancies in corneal ulcer readings and monitoring the clinical response to therapy. [14]

Another clinically detectable condition through AI algorithms is the corneal rejection of the transplanted graft after Descemet membrane endothelial keratoplasty (DMEK). However, distinguishing cases where rejection will resolve spontaneously from those requiring further surgery by injecting an additional air bubble into the anterior chamber is challenging. As described by Hayashi and colleague's neural networks could facilitate the identification of individuals deserving additional treatment. [15]

The ocular surface disease known as pterygium is characterized by abnormal conjunctival growth that encroaches into the cornea. Artificial intelligence has been

proposed in this situation to discriminate between eyes with pterygium and those that are normal. [16, 17, 18]

1.1.1.2 Lens

Cataract, which affects 12.6 million people globally and is the primary avoidable cause of blindness, is the principal lens-related condition. This number will increase because of the population's continued ageing and inadequate healthcare, particularly in low-income countries, which causes a discrepancy between the demand for surgery and its availability and, as a result, in longer surgical waiting periods. [19, 20]

The three main types of cataracts in adults are nuclear, cortical, and posterior subcapsular. Currently, slit-lamp examination is used for screening and diagnosis. The grading methods like the Lens Opacities Classification (LOCS) III and the Wisconsin Cataract Grading System are used to determine the cataract severity. [21, 22]

With slit-lamp imaging and fundus photography, many research teams studied the potential use of AI technology to automatically diagnose and categorize cataract severity. [23] Initial studies, such as the one conducted by Wu et al., achieved an AUC>0.99 in differentiating between the presence of artificial lenses (IOL), normal lenses, and cataracts on slit-lamp images and an AUC>0.91 in staging the severity. [24]

In addition to the aforementioned uses, AI can also be useful in areas related to cataract surgery, such as measuring corneal power after laser refractive operations and calculating IOL power using biometry. [25, 26]

1.1.1.3 Irido-Corneal Angle and Associated Structures

The iridocorneal angle is an important ocular structure, and if its width is reduced, it can lead to closed-angle glaucoma. In general, open-angle and closed-angle glaucoma rank as the third most prevalent cause of blindness worldwide. [19] Among the two types, the one that leads to greater and more severe vision loss is the latter. Patients are asymptomatic until an acute iridocorneal angle occlusion occurs. Therefore, it's critical to identify those who are at risk to stop the progression of glaucoma. [7]

Clinical diagnosis is based on gonioscopy. [27] However, this method lacks reliable repeatability and is sensitive to subjectivity. Alternative methods are employed to create

a more impartial frame of reference, including UBM, anterior segment OCT, and tonometry employing Scheimpflug Technology (Pentacam). [28, 29] While gonioscopy records sensitivity within a range of 44.4% to 49.5% for the identification of closed angles, AS-OCT demonstrates levels of sensitivity ranging from 88.4% to 98.0%. However, AS-OCT has low specificity (12%-87%), leading to over-treatment and unnecessary follow-up controls. [30, 31] Compared to gonioscopy, OCT can identify the causative mechanisms of angle closure through retinal scans. The four main mechanisms leading to angle closure are:

- Increase in the diameter of the lens
- Pupillary block
- Increase in peripheral iris thickness
- Plateau iris

Finding the exact mechanism is crucial for patient care since each mechanism demands a certain course of action. [32]

AI has been applied in the screening of closed-angle glaucoma using images from OCT, demonstrating high accuracy in this task. [7] Xu et al. created an algorithm that correctly recognized angle closure in AS-OCT images with an AUC of 0.93 to 0.95. [33] In a second study, Fu et al. realized a VGG-16 DL system to distinguish between closed-angle glaucoma and its absence using AS-OCT images. [34] According to their research, the AUC ranged from 0.90 to 0.96, the sensitivity from 79% to 93%, and the specificity from 87% to 91%. [34]

1.1.2 Posterior Segment

DL has been utilized by several researcher to identify early signs of retinal disorders in OCT images such as glaucoma, age-related macular degeneration (AMD), macular edema, and diabetic retinopathy (DR). [35-40]

1.2 OCT

Without any physical contact, OCT generates high-resolution cross-sectional images of the tissues under investigation. For organs like the human eye, where traditional microscopic tissue examination by biopsy is very tricky, this is very helpful. [41] The

fast signal processing and quick scanning of OCT enable real-time image visualization. [42]

There are two primary OCT approaches: The two basic categories of OCT technology are Time-Domain (TD)-OCT and Frequency-Domain (FD)-OCT. The latter includes the subsets Spectral-Domain (SD)-OCT and Swept-Source (SS)-OCT. [43]
TD-OCT requires depth scanning for each position, resulting in slow imaging speed acquisition and poor image quality. Due to these limitations, its use remains restricted. Conversely, FD-OCT acquires depth information, improving image quality and examination speed. Like TD-OCT, SD-OCT uses a broadband light source, but several photodetectors are used to increase sensitivity. Contrarily, Swept-Source (SS)-OCT uses a narrowband laser source to combine the sensitivity reached by SD-OCT with the hardware simplicity of TD-OCT. [42]

Confocal scanning laser ophthalmoscopy (cSLO) and SD-OCT, two complementing imaging technologies, were combined to create the SPECTRALIS system, introduced by Heidelberg Engineering in 2006.
A variety of laser sources that offer various illumination wavelengths and detection patterns make up the cSLO component of SPECTRALIS. These include infrared (IR), green, and blue cSLO reflectance imaging. It also offers fluorescein angiography (FA), indocyanine green angiography (ICGA), and autofluorescence (blue and IR angiography, or infrared angiography).

OCT and confocal IR imaging are frequently combined, however alternative pairings are feasible. Confocal imaging generates a cross-sectional retinal image that lines up with the OCT's en-face plane, enabling flexible camera positioning to capture the desired retinal area. The smooth capture and quality control throughout the inspection are made easier with real-time image presentation. The cSLO image and the OCT image are simultaneously recorded. (Figure 1.1)

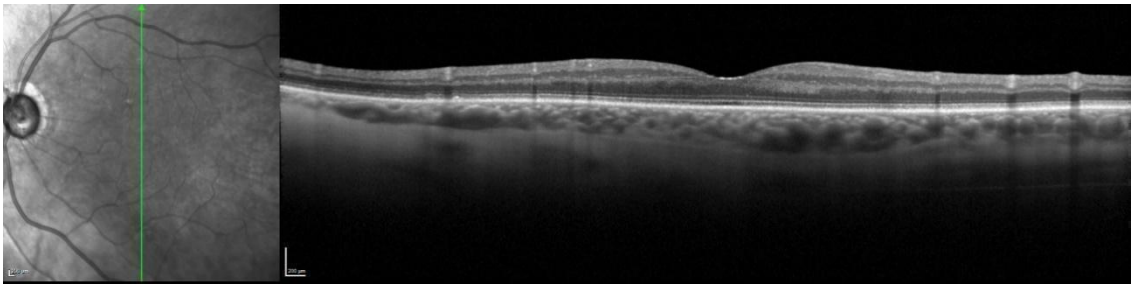

Figure 1.1: Example of an image acquired with Spectralis, left eye (OS).

The ability to co-register OCT and cSLO images enables follow-up exams to be performed in the exact same spot on any subsequent visit. Active eye tracking (TruTrackTM), which continually detects movements inside the cSLO image and readjusts the OCT beam accordingly, is used to provide this capacity. The automatic tracking of motion and the overlay of images acquired on the same patient at different times allow monitoring of any alterations in the studied retinal portion. [42]

Similar to ultrasound OCT can obtain three different types of images: A, B, and C-scan:

- ***A-scan*** images, or one-dimensional scans, analyze the reflectivity and depth of structures along a single light beam. They are rarely used, mainly for accurately measuring eye length.
- ***B-scan*** images, or two-dimensional scans, are obtained by juxtaposing around 1600 A-scan scans along a line of approximately 6 mm length. They are the most frequently used representations in ophthalmology and closely resemble histological tissue sections.
- ***C-scan*** images are three-dimensional reconstructions composed of many adjacent B-scan sections.

1.3 OCT and Maculopathy Signs

In posterior segment pathologies, various signs can be observed through OCT examination.

1.3.1 Drusen

Histologically drusen are characterized by lipid, protein, and cellular debris aggregations and they are localized between the inner layer of Bruch's membrane (BM) and the basal lamina of the retinal pigment epithelium (RPE). At the fundus examination they appear as yellow patches. It's common for these subepithelial deposits to appear with ageing, albeit they might not always be a sign of disease. However, the likelihood of developing AMD might vary depending on their number, location, and type. [44-46]

There are many types of drusen, and their sizes, consistency, and histological characteristics are useful to categorize them.

- ***Hard drusen***, which are often seen during the ageing process and are thought to be normal. They are tiny, rounded deposits having a diameter of less than 63 microns.
- ***Soft drusen*** are less distinct deposits with a diameter more than 125 microns. [45] The larger drusen are thought to obstruct the exchange of nutrients and waste materials between the choroidal blood veins and the retina. [47] This lack of metabolic exchange ultimately leads to retinal atrophy and degeneration, a degenerative condition connected to AMD.

Cuticular drusen, sometimes referred to as punctate drusen, range in size from 25 to 75 microns. They frequently group together and are typically numerous, gradually generating bigger deposits. The central and peripheral retinas both have drusen, both hard and cuticular. Nevertheless, they are localized mostly in the macular area.

According to one idea, the division made by soft drusen between BM and the RPE may encourage the growth of macular neovascularization along this line. This may account for the increased risk of AMD developing from soft drusen. [45]

Drusen are most frequently linked to AMD, however it's important to understand that they are not just related to AMD. More uncommon genetic diseases such Sorsby's dystrophy, Stargardt's disease, adult-onset vitelliform macular dystrophy and North Carolina macular dystrophy can also cause similar deposits that resemble drusen. [46]

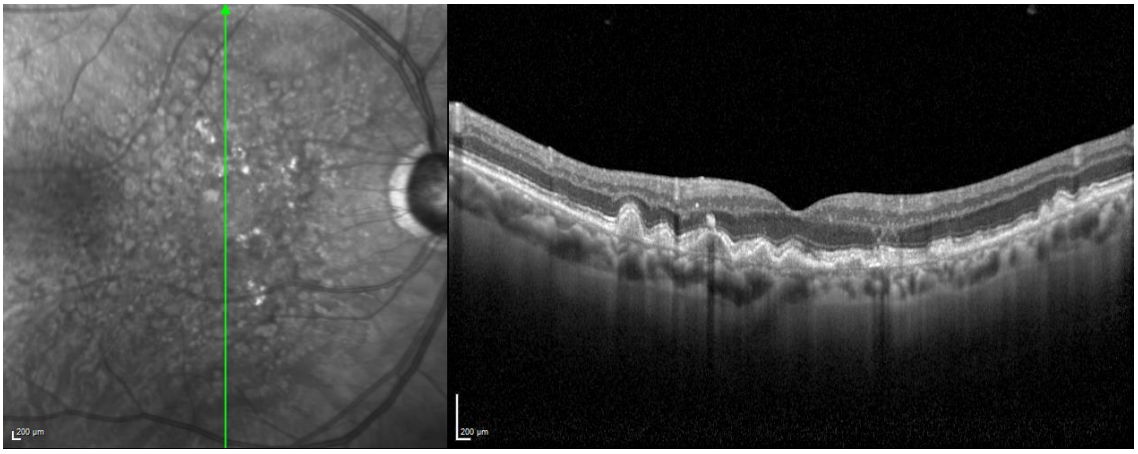

Figure 1.2 OCT scan containing drusen, right eye (OD).

1.3.2 Intraretinal and Subretinal Fluid

The presence of fluid at the intraretinal and subretinal layers is linked to ocular illnesses such AMD, DR, and retinal venous occlusion. (Figures 1.3 and 1.4). OCT is used to monitor the distribution and amount of intraretinal and subretinal fluid, which manifests as areas with diminished reflectivity, in order to assess the severity and progression of these disorders. [47, 48]

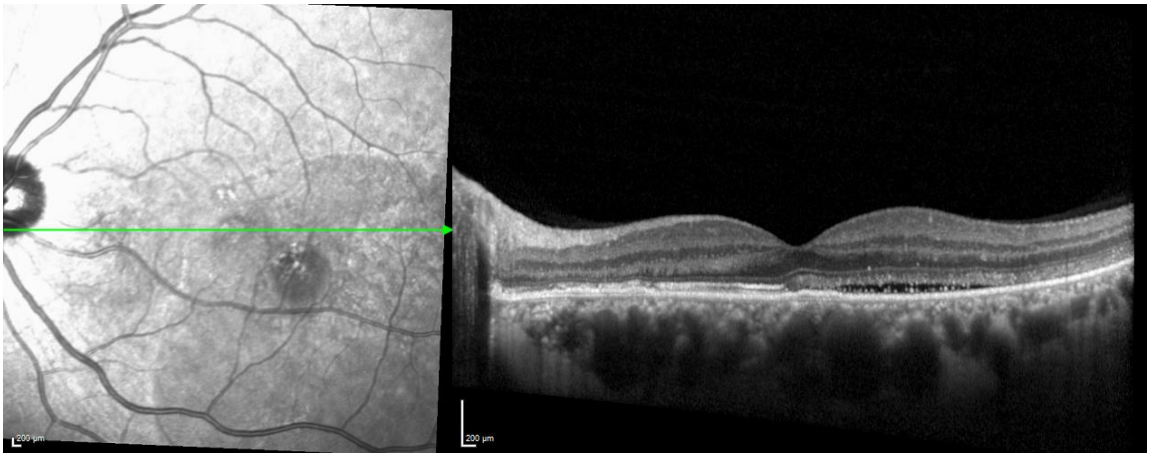

Figure 1.3: OCT scan containing subretinal fluid, left eye (OS).

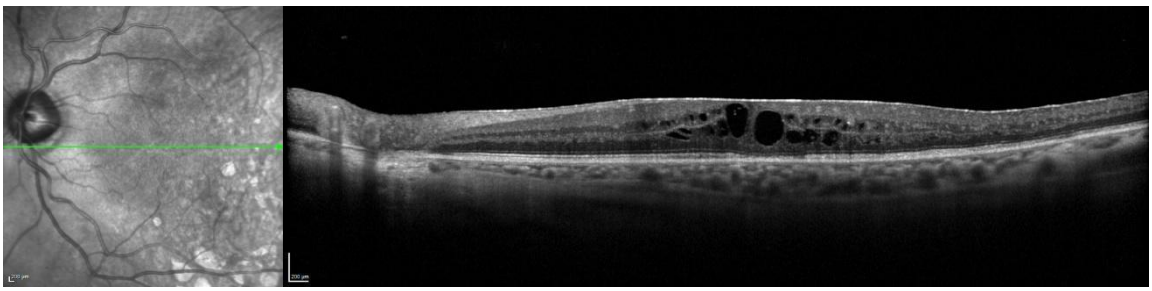

Figure 1.4: OCT scan containing intraretinal fluid, left eye (OS).

1.3.3 Macular Neovascularization

Macular neovascularization (MNV) is characterized by the development of new blood vessels linked to the choroidal vessels. These vessels are located between BM and the RPE. [49] (Figure 1.5) The new vessels can involve both peripheral retinal portions and the sub foveal zone. Bressler et al. found that peripheral MNVs are more correlated with pathologies other than AMD, whereas sub foveal MNVs are mostly observed in subjects with AMD. [81] BM disruptions are a frequent sign of diseases associated with MNV in clinical practice. However, it is still unclear how exactly these disruptions contributed to the growth of neovascularization. [50] Due to BM discontinuities, the evolution of MNV involves fluid seeping beneath the RPE. This may lead to a disciform scar developing or a serous retinal detachment [51, 52].

Based on the anatomical position there are four MNV types:

- ***Type 1:*** it's characterized by neovascular proliferation under the RPE.
- ***Polypoidal choroidal vasculopathy***: presence of a network of branching choroidal vessels with small aneurysmal dilations or projections called polyps.
- ***Type 2:*** neovessels developed in the subretinal space above the RPE are referred to as type 2 MNV.
- ***Type 3:*** an anastomosis between the choroidal and retinal circulations develops when the retinal circulation is damaged; sometimes called retinal angiomatous growth. [53]

The gold standard for MNV diagnosis is fluorescein angiography. In people who already have neovascular AMD in their other eye, studies have shown that both OCT and OCTA

showed a high level of accuracy and specificity in recognizing newly generated MNVs in the partner eye. [54, 55]

1.3.4 Backscattering

In physics, backscattering (BS) corresponds to retro diffusion, which is the backward scattering of matter, radiant energy, or particles, at a scattering angle of 180°.

The light waves traveling through the ocular tissues can either be reflected, dispersed or absorbed when they reach different surfaces within the tissue while making OCT images. Each retinal layer has different reflective, diffusive, and absorptive properties. [56]

The angle at which the backscattered light reaches the region of concern directly affects the quality of the illumination. Because of this, structures inside the retina with an oblique orientation, such as the layer of Henle's fibers, may not be clearly visible or may have different appearances in OCT images. [57] Reflectivity is represented in shades of gray: if it tends towards black, it means the tissue is less reflective, whereas if it tends towards white, it is hyper-reflective. [58]

Going from the most surface-level to the deepest layer, these are the layers that are typically visible in an OCT image of a healthy patient:

- Posterior hyaloid
- Internal limiting membrane
- Nerve fiber layer
- Ganglion cell layer
- Inner plexiform layer
- Inner nuclear layer
- Outer plexiform layer
- Outer nuclear layer
- External limiting membrane
- Photoreceptor layer
- Pigmented epithelium

The choroid is divided into two layers: the Sattler layer, which houses medium-sized vessels, and the Haller layer, which houses bigger vessels. The choroid is located underneath the complex of pigmented epithelium and BM. [56]

The EPR abnormalities can be observed with OCT. For instance, focused areas with missing or depigmented epithelium have increased choroidal vessel reflectivity. This sign is referred to as BS. Additionally, pigment aggregation and migration, such as elevations of the pigmented epithelium caused by drusen, can be seen as foci of hyper-reflectivity with underlying shadows.[59]

The causes of loss or atrophy of the EPR are several. Dry AMD degeneration evolving into geographic atrophy (GA) gives rise to BS, but areas of atrophy of smaller extent are sufficient to observe this sign, such as those generated by laser photocoagulation. [56, 60]

1.3.5 Epiretinal Membrane (ERM)

A macular abnormality called epiretinal membrane (ERM), which appears on the retina's external limiting membrane, is rather prevalent. The incidence is between 7% and 11.8%, and the frequency rises with age. [62, 63]

ERMs are classified into secondary to ocular diseases and primary, which are idiopathic. [63] The main causes of secondary forms are previous cataract surgery, DR, and retinal venous occlusion.

In many cases, ERM is asymptomatic but depends on location and type of the membrane. When the macular or peri-macular area is damaged, it can result in additional abnormalities like macular edema and retinal traction, as well as blurred vision, decreased visual acuity, metamorphopsia, loss of stereopsis, and aniseikonia. [64]

The clinical classification based on fundus examination was first proposed by Gass: *Grade 0* corresponds to the presence of macular cellophane without retinal distortion; *Grade 1* corresponds to the appearance of retinal distortion with wrinkling of the cellophane; *Grade 2* is defined as macular pucker with denser ERM, grayish appearance, and marked retinal distortion. *Grade 3* is represented by the formation of a pseudo hole, caused by the traction exerted by ERM. [65] Today, this classification has been surpassed by others based on OCT.

Clinical observations and an OCT examination both contribute to the diagnosis of ERM. In OCT imaging, an amorphous, hyper-reflective layer on the internal limiting

membrane (ILM) identifies ERM. It typically coexists with hypo reflective zones between the ERM and ILM, as well as retinal radial folds. [66]

1.3.6 Macular Hole

Macular Hole (MH) is a defect in retinal tissue that extends through its full thickness and affects the fovea. The pathogenesis can be traumatic, but it has been observed that most are of idiopathic, without a clear etiopathogenic mechanism. [67]

Gass's biomicroscopic classification comprises four stages:

- ***Stage I.A and I.B***: disappearance of the foveal depression and thickening of the retinal profile. No vitreous separation.
- ***Stage II***: Full-thickness MH with partial adherence of the retinal operculum. No vitreous separation.
- ***Stage III***: Full-thickness MH without adherent operculum and diameter less than 400 µm. No vitreous separation.
- ***Stage IV***: Full-thickness MH without adherent operculum and diameter greater than 400 µm. Complete vitreous separation. [65]

Lamellar MHs and pseudo-holes, which are brought on by an ERM, are the two disorders that most frequently resemble full-thickness MHs.

Lamellar holes, which are limited to the macular area, are partial abnormalities in retinal thickness. They may be a side effect of cystoid macular edema or arise from a full-thickness hole not fully formed. They show as flat, crimson, well-defined lesions at the fundus examination. [68,69].

The lamellar hole can sometimes be associated with an ERM, causing tangential traction on the retinal layers, interrupting them. [70]

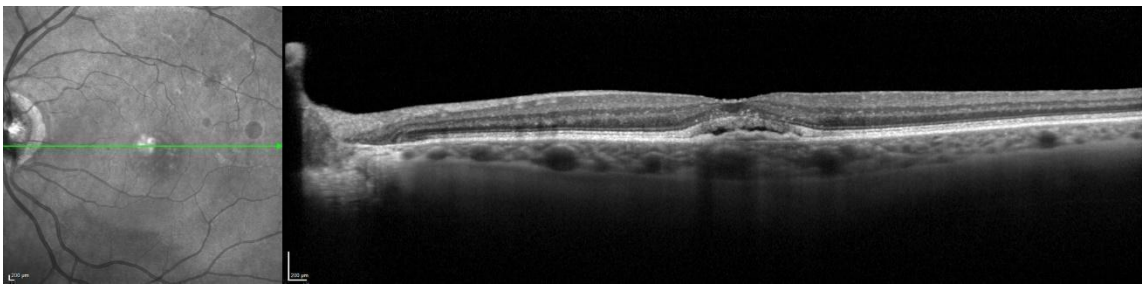

Figure 1.5 OCT scan containing MNV, left eye (OS).

1.4 Major retinal pathologies related to OCT signs

1.4.1. Diabetic Retinopathy

In many industrialized countries, DR continues to be the predominant cause of vision impairment due to the global growth in diabetes mellitus prevalence. [71] Although diabetes can have a variety of negative effects on the eyes, such as increasing the incidence of cataracts, DR emerges as the most common and serious disease, affecting around one-third of people with diabetes. [71, 72] The following are risk factors for DR:

1. Non-modifiable:

- *Onset age*
- *Duration of the disease*
- *Genetics (family history and ethnicity)*
- *Type 1 Diabetes*

2. Modifiable:

- *Hyperglycemia*
- *Arterial hypertension*
- *Lipid profile*
- *Cataract surgery*
- *Pregnancy*

Additionally, epidemiological research has shown that DR, especially in less severe presentations, is linked to an increased risk of systemic vascular conditions such as heart failure, coronary artery disease, and stroke. [73] Independently from traditional cardiovascular risk factors, this connection persists. [74–76] These results suggest that substantial microcirculatory damage in diabetics is signaled by the development of retinopathy, highlighting the significance of careful cardiovascular monitoring for patients with DR. [77]

The core of the pathogenesis is the hyperglycemia-induced retinal microangiopathy, leading to alterations in the capillary walls. On one hand, there's an increase in vascular permeability and fragility, leading to edema and tissue hemorrhages; on the other hand, there's a reduction in capillary diameter and capillary closure, leading to retinal ischemia and subsequent release of angiogenic substances and neovascularization. Anomalies in brain tissue, in addition to vascular alterations, contribute to the emergence of DR. Diabetes-related neural problems, such as axonal degeneration and neuronal cell death, are permanent and strongly associated with reduced eyesight. [78, 79]

The most prevalent reason for diabetics' diminishing visual acuity is diabetic macular edema (DME), which can appear in any kind of DR. The main factor causing DME's complex and difficult pathophysiology is the blood-retinal barrier rupture. The intercellular gaps get clogged with macromolecules and fluids. [80]

The Early Treatment Diabetic Retinopathy Study (ETDRS) and the International Clinical Diabetic Retinopathy (ICDR) are the two main clinical categorization systems used for DR classification. [81-82] These classifications include several types of DME and group them according to whether neovascular growth is present or not.

1. ***Non-proliferative***, further divided into mild and moderate
2. ***Pre-proliferative***
3. ***Proliferative***, distinguished as high-risk when significant vascular proliferation is present.

Various diagnostic investigations are used to classify DR. The main are [83]:

- *Visual acuity examination*: however, visual acuity is not initially compromised, so further investigations are necessary.
- *Ophthalmoscopy* (fundus examination): this is the best way to prevent and diagnose diabetic retinopathy.
- *Retinal Fluorescein Angiography*: Microaneurysms and increased capillary permeability are the first noticeable changes in DR. Macular ischemia is indicated by the growth of the avascular foveal area, whereas focal patches of capillary non-perfusion suggest retinal ischemia. The leaking of dye into the vitreous can be used to detect the existence of retinal neovascularization. The two main angiographic patterns for diabetic macular edema are localized (caused

by leaky microaneurysms) and diffuse (coming from a widespread breakdown of the blood-retinal barrier).

- *OCT:* Used to study different retinal layers, particularly for detecting retinal edema, which is not easily visible through ophthalmoscopy. For tracking the progression and assessing the efficacy of treatment for diabetic macular edema, this approach offers precise and reliable measures of retinal thickness. It also helps in spotting structural changes (such vitreomacular traction or ERM).
- *Ultrasound*: An advanced diagnostic examination used when the eye fundus cannot be visualized, usually due to significant bleeding or cataracts.
- *Iridography*: An angiography of the iris vessels, useful as neovascularization involves both retinal vessels and those in the iris;

Most lesions associated with DR are found in the posterior pole, within the vascular arcade, at the nasal side. Lesions can be linked to:

- Consequences of increased vascular permeability: macular edema, hard exudates, retinal hemorrhages.
- Consequences of ischemia and neovascularization: microaneurysms, venous and arterial alterations, abnormal neovascularization, preretinal and/or vitreal hemorrhages.
- Consequences of infarction: cotton wool spots or soft exudates.

1.4.1.1 Non-Proliferative Retinopathy

Non-Proliferative Retinopathy is characterized by the absence of neovessels. This form might be further divided into mild and moderate. [81, 82] The first sign of the mild form is the presence of microaneurysms, which are sac-like dilations on the venous side of retinal capillaries. They are difficult to see during ophthalmoscopic examination, when visible, they appear as small red dots, sometimes indistinguishable from minor hemorrhages, but are clearly outlined during fluorescein angiography as they fill up with dye. Microaneurysms are the earliest sign but not pathognomonic, as they can also be found in other conditions like hypertension. [84] Microaneurysms form due to alterations in the retinal capillary walls; these capillaries become more fragile, increasing the risk of hemorrhages. [85]

Retinal hemorrhages can be superficial or deep. Superficial hemorrhages have a flame-shaped appearance, while deeper ones tend to be rounder. [85]
Non-proliferative retinopathy becomes moderate when hard exudates appear; they are well-defined yellow-white deposits of lipoproteins on the retina. [81, 82] They form due to retinal edema, where fluid and large molecules leak out of capillaries. The fluid is reabsorbed, while the molecules deposit and accumulate on the retina, forming hard exudates. These structures have a "circinate" arrangement, circular in shape, with the capillary at the center of the circle, followed by edema and deposits at the periphery. This element is always present as it arises from capillaropathy; it can appear at the beginning of the disease without microaneurysms (a very rare condition) or emerge in advanced stages. [81, 82]

1.4.1.2 Pre-Proliferative Retinopathy

Characterized by more significant alterations compared to the non-proliferative form, yet without neovascularization. These alterations include:

- ***Venous caliber anomalies***: venous vessels no longer have a straight shape but appear twisted, tortuous, dilated.
- ***Intraretinal Microvascular Abnormalities (IRMA)***: Capillaries begin to deform and twist (localized capillary dilations, tortuous and ecstatic capillary segments). These aren't neovessels but rather pre-existing capillaries. They have an altered wall, allowing fluid to escape and form macular retinal edema. Arteriovenous shunts are formed, visible as fine and irregular red lines from arterioles to venules.
- ***Microaneurysms***, more numerous than in the non-proliferative form.
- ***Deep and diffuse retinal hemorrhages***.
- ***Soft exudates***, round or oval-shaped, more white and less defined compared to hard exudates, also known as "cotton wool spots", due to their indistinct margins. They are small infarcts (ischemic necrosis) of nerve fibers, mainly located at the edges of recent ischemic areas.
- ***Retinal ischemia***: This condition characterizes pre-proliferative retinopathy and precedes neovascular formation. The ischemic phase is hard to detect ophthalmoscopically, but it can be identified using fluorescein angiography by pinpointing occluded vessels that lead to ischemic damage. Capillary occlusion

can result in large completely ischemic areas, with dilated, anomalous, and frequently shunted capillaries at the margins. Ischemia triggers the release of angiogenic substances (VEGF, FGF, IL8, IGF1), preceding neovascular formation. Neoangiogenesis is visible as ectasis at the borders between perfused and ischemic zones. This mechanism is activated to compensate for the lack of perfusion. Neovascularization is uncoordinated and anarchic: a subpar attempt since the neovessels have thin and fragile walls, and instead of nourishing the ischemic area, they can rupture and cause hemorrhages. 40% of patients with pre-proliferative retinopathy (with ischemia) progress to proliferative retinopathy within 12 months. [81, 82]

1.4.1.3 Proliferative Retinopathy

Characterized by significant neovascular formation and growth, stimulated by ischemia. These neovessels have very thin walls, making them particularly fragile. They can easily rupture, causing bleeding, and induce the formation of fibrotic tissue around them. This process is called fibrovascular proliferation. Neovessels form on the retinal surface, both near the optic nerve and in the vitreal cortex, and then spread diffusely across the retinal surface, leading to an advanced pathological state. Neovessels can be seen in fluorescein angiography as light spots on capillaries, highlighting dye leakage. [73, 81]

Fibrovascular proliferation is due to the marked permeability of the vessel walls, leading to the extravascular loss of proteins, fibronectin, and other substances, activating fibroblasts that start producing collagen, thus creating fibrotic tissue around neovessels. This tissue anchors neovessels to the vitreal cortex and retina, exerting traction on the surrounding retinal tissue. This condition can also lead to tractional retinal detachment, a typical complication of this form of retinopathy, with catastrophic visual consequences. [73] Another complication is bleeding caused by neovessel rupture. The resulting hemorrhages can take various forms, such as the "boat-shaped" hemorrhage located between the retina and the posterior hyaloid. [86]

Neovascular glaucoma is the most severe consequence that can result from proliferative DR. Angiogenic factors don't remain confined to the vitreous but also reach the anterior chamber, stimulating neovessel growth there as well. They can develop on the iris and in the iridosclerocorneal angle, leading to angle-closure glaucoma. These are severe forms of glaucoma, often untreatable, ultimately causing blindness. [73]

As a result, the following are the primary reasons for significant vision loss in DR:

- Diabetic maculopathy, namely macular edema
- Vitreous hemorrhage
- Neovascular glaucoma
- Tractional retinal detachment

However, the condition can be asymptomatic if it doesn't involve the macular area; for this reason, symptoms cannot be correlated with the stage of retinopathy. [87]

1.4.1.5 Treatment

The primary treatment for DR is prevention, achieved through metabolic and glycemic control. [88, 89] All diabetics should undergo screening to monitor various changes that may indicate the onset of the condition. Screening is conducted through fundus examination with a slit lamp (direct ophthalmoscopy) and retinal photography, which captures images of the eye's fundus. The screening intervals are determined based on risk factors and the stage of retinopathy. [90]

For diabetic patients, controlling blood pressure is crucial in preventing retinopathy. There is a 10% to 15% increased risk of developing proliferative retinopathy for every 10 mmHg increase in systolic blood pressure, as well as a 10% to 15% increased risk of developing early DR. [91, 92]

Systemic agents promoting intensive glycemic control, dyslipidemia control, and renin-angiotensin system antagonists (antihypertensives) have shown beneficial effects on DR. [93]

There are targeted molecules for diabetic patients with DR; however, this systemic medical therapy is still under investigation and currently not a valid treatment. Drugs like protein kinase C inhibitors (like ruboxistaurin) or somatostatin analogues (like octreotide) either orally or intramuscularly have not produced the required results in controlled prospective trials. [94, 95]

There are two types of laser photocoagulation: [96]

- ***Focal laser photocoagulation***: small burns are created on the retina to destroy the altered capillaries responsible for macular edema formation. This is used to treat macular edema.

- ***Panretinal laser photocoagulation***: used for proliferative diabetic retinopathy treatment. The goal is to destroy ischemic areas to block the release of angiogenic substances, thus halting the development of new vessels. This treatment is still employed. If the ischemic areas are extensive and neovascularization is present at multiple points, the laser treatment is not focused solely on them, but a panretinal photocoagulation is performed. This treatment is less conservative as it significantly reduces the patient's visual field but prevents blindness caused by retinopathy.

The current therapy used for macular edema treatment, alongside focal laser photocoagulation, is intravitreal injection therapy with anti-angiogenic drugs, inhibiting factors promoting angiogenesis. VEGF not only induces angiogenesis but also increases vascular permeability; therefore, these drugs avoid retinal angiogenesis and retinal edema. Intravitreal cortisone injection, used solely in macular edema treatment, is also an option. [96, 97]

In advanced situations, surgical intervention is considered as a last approach. When proliferative retinopathy-related problems such recurrent vitreous hemorrhage or tractional retinal detachment occur, vitrectomy is required. Surgery can still be used to stop the disease's progression towards blindness even if the prospect for functional improvement may be limited at this point in the disease's course. [98]

1.4.2 Age-related macular degeneration

A macular disorder called AMD leads to deterioration of central vision. It is a significant factor in visual impairment, causing severe vision loss and blindness. [99] According to population-based study, among those aged 55 to 64, the prevalence of AMD is predicted to be 0.2% (10 out of 4797 participants). [100] For people 85 years old and older, this percentage dramatically increases to 13.1% (68 out of 521).

Traditionally, the diagnosis of AMD was based on fundus examination with a slit lamp. Over the past two decades, advancements in technology and the development of new imaging modalities have supported diagnosis through OCT, fundus autofluorescence (FA) and angiography. MNV in neovascular AMD may still be found using contrast-enhanced angiography, which also helps to locate it precisely and gauge its activity. On the other hand, a brand-new, non-invasive imaging technique called optical coherence

tomography angiography (OCTA) can produce volumetric angiographic images in few seconds. Contrast agents are no longer necessary thanks to OCTA, a dye-free, non-invasive alternative. However, it identifies the presence of macular neovascular networks but does not detect any leakage. [99, 101]

1.4.2.1 Risk Factors

Risk factors can be classified into two categories:

- *Non-modifiable*: Age, ethnicity, family history, female gender, iris color (higher risk in light irides). Age is the strongest risk factor, particularly above 60 years of age. Caucasians are more affected compared to African and Asian populations.
- *Modifiable*: The primary factor is retinal tissue oxidation, which can be counteracted with antioxidant agents taken as dietary supplements. Smoking and alcohol consumption are oxidative risk factors. The role of arterial hypertension, lipid profile, and obesity, which do not seem to be implicated in this condition, remains unclear. [102, 103]

1.4.2.2 Pathogenesis

The retina, an essential element of vision, lines the inside rear wall of the eye, it is constituted centrally by the macula which has the function of fine vision and color perception. The fovea, which is centrally placed inside the macula, is crucial in maintaining fundamental visual abilities required for daily tasks. The BM, the RPE and the underlying choroidal capillary and choroid layers all experience notable effects in the setting of AMD. RPE and choroidal capillaries are extensively impacted by AMD, particularly when neovascular lesions form. The photoreceptor layer, where rods and cones interact in the complex process of phototransduction, a crucial component of visual function, is nourished by the RPE in a crucial way. AMD is characterized by RPE dysfunction and atrophy, which negatively affect the health of the photoreceptor layer and interfere with phototransduction. Loss of vision is the end outcome of this dysfunctional process that prevents signals from the retina from reaching the brain.
The vascularization of the choroid is thought to be impacted by the microvascular damage caused by some systemic diseases, including hypertension and hyperlipidemia. [104] The aberrant expression of certain VEGF subtypes is triggered by hypoxia, which

leads to the growth of new choroidal capillaries that are susceptible to the unique hemorrhaging and leaking seen in neovascular AMD. [105]

In conclusion, there are essentially four elements that contribute to AMD

1. Photoreceptors
2. RPE
3. BM
4. Choroidal Capillary Layer

Aging of retinal tissue, genetic factors, and certain environmental factors inducing oxidative processes result in alterations of the above-mentioned morpho-functional unit.

1.4.2.3 *Classification*

There are several classification techniques used to categorize AMD. AMD is often divided into early and late phases in epidemiological study. The Age-Related Eye Disease Study (AREDS) severity scale and its abbreviated form are commonly used in clinical and experimental studies. [99]

The basic clinical classification distinguishes between:

- ***Early AMD***: presence of drusen between 63 µm and 125 µm, without pigment abnormalities.
- ***Intermediate AMD***: presence of drusen > 125 µm or any pigment abnormality.
- ***Late AMD***: neovascular form or GA. [106]

The simplified AREDS severity scale points are:

1. No drusen > 125 µm or pigment abnormalities in both eyes.
2. Large drusen or pigment abnormalities in one eye.
3. Large drusen or pigment abnormalities in one eye; or large drusen or pigment abnormalities in both eyes; or neovascular AMD or GA in one eye.
4. Large drusen or pigment abnormalities in one eye and large drusen or pigment abnormalities in the other eye.
5. Large drusen or pigment abnormalities in both eyes. [107]

AMD is categorized using additional morphological features, with a particular emphasis on the presence or absence of aberrant choroidal vascular growth or atrophy. [104]

If the situation is stable, early, or intermediate dry AMD varieties may show a more encouraging prognosis. It is important that there is a 10% to 15% chance of exudative AMD developing during the illness for all kinds of dry AMD. [108] Additionally, wet AMD may progress to GA or vice versa. [109]

1.4.2.3 Dry AMD

Dry AMD is the most common type of AMD (90% of cases). Initially, visual acuity is normal, but over time and with increasing degenerative phenomena, it decreases. It is usually bilateral and asymmetric.

Characteristic alterations of this form include: [104]

- Drusen
- RPE
- GA
- Drusenoid detachments of the RPE

Drusen are areas of extracellular lipofuscin material that may be seen in OCT images and are located between BM and RPE. They appear to result from the accumulation of debris formed during phagocytosis by RPE cells of the outer segment of photoreceptors. [45]

There are two types of drusen:

- ***Hard drusen***: small, yellowish dots, smaller lesions, pinpoint, well-defined edges.
- ***Soft drusen***: larger, with more diffuse edges, lighter in color, often confluent. Accumulating beneath the RPE, they can lead to a detachment called drusenoid detachment. This predisposes to the appearance of capillaries, indicative of progression toward the exudative form. [104]

They can have different sizes, volumes, and numbers. These manifestations can be seen clearly with multimodal imaging, particularly when OCT is used to determine the size, location, and extent of drusen. [101]

Pigment abnormalities of the RPE result from cellular disorganization: some cells are lost while others proliferate, leading to a remodeling of the epithelium that no longer has a homogeneous coloration. [104]

GA is so named due to irregular borders and is characterized by complete atrophy at the macular level involving the choroidal capillary, RPE cells, and overlying photoreceptors. It represents the final stage of dry maculopathy, resulting in significantly reduced visual capacity. The damaged central zone is approximately 4 mm in diameter, causing the patient to have a central scotoma while retaining the rest of the visual field. [110]
The borders and extent of the lesion can be quantified more accurately using FA and OCT, allowing for the detection and monitoring of GA progression. [111]

1.4.2.4 Wet AMD

The most frequent advanced form of AMD is exudative or neovascular AMD, sometimes known as "wet" AMD. Without treatment, fibrosis and permanent vision loss ensue from hemorrhaging and fluid seepage caused by the formation of neovascularization into the retinal layers or subretinal space. [104]

Neovessels originate from the choroidal capillary and first extend beneath the RPE and then, following RPE rupture, beneath the retina. Neovascular AMD can be classified into three types, as described earlier. In addition to visual acuity reduction, other symptoms associated with neovascularization and retinal edema include metamorphopsia, i.e., distorted vision of images, and the presence of macular scotoma. [104]

The Amsler grid test (Figure 1.6) is used for diagnosing metamorphopsia, especially in patients with initial maculopathy, to promptly recognize the shift to the neovascular form. Therefore, it is important to identify even subtle metamorphopsia. The patient is instructed to fixate on the central point of the grid. If they begin to perceive the grid abnormally or notice changes from day to day, it would be a sign of metamorphopsia. [112]

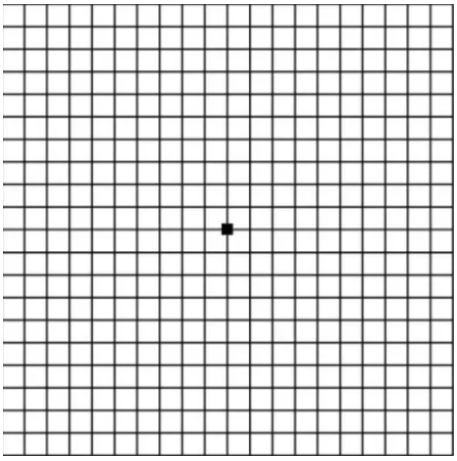

Figure 1.6: Amsler Grid, used for the identification of metamorphopsia.

1.4.2.5 Treatment

Dry AMD is due to oxidative processes, thus, like other conditions, antioxidant-based supplements can be useful. This type of treatment, in the context of AMD, has been scientifically evaluated through studies lasting several years.

Guidelines for vitamin supplementation were provided by the Age-Related Eye Disease Study (AREDS), which also showed a 25% decrease in the development of advanced AMD. Zinc, vitamin C, vitamin E, lutein, and zeaxanthin are among modern supplements. [113] The AREDS2 formulation replaced beta-carotene, which was previously included, with lutein and zeaxanthin owing to the increased risk of lung cancer in smokers. However, its efficacy has not been shown in individuals with early AMD in both eyes. It is advised to supplement for patients with intermediate or early AMD in one eye and advanced AMD in the other. For the goal of prevention, it is not advised. [113]

A change in lifestyle is suggested for all patients. These adjustments include dietary modification that emphasize the consumption of foods high in antioxidants, omega-3 fatty acids, and omega-6 fatty acids, particularly seafood. In addition, managing your weight and quitting smoking are advised behaviors. [104] Other modifiable risk factors must also be addressed, such as lowering cholesterol and blood pressure.

There is conflicting evidence about how UV exposure affects the onset of AMD. However, one lifestyle change you might think about is reducing your sun exposure. [114]

For wet AMD, possible treatments include [104]:

- ***Physical therapy***: before the 2000s, laser photocoagulation was the cornerstone of wet AMD therapy. Targeted thermal energy was used on the neovascular membranes, inducing their scarring. The limitation of this technique is the occurrence of scotoma and permanent vision loss in the treated area.
- ***Photodynamic therapy (PDT)***: Verteporfin is injected and exclusively binds to the neovascular endothelium. It is then irradiated with a low-intensity diode laser to achieve coagulation only at the level of neovascular membranes. This allowed for the first time the elimination of neovascular membranes without destroying the overlying retina.
- ***Medical therapy***: Involves intravitreal treatment with anti-VEGF drugs. The adverse effects of these medications, which are given as outpatient injections, are quite low. One of the first mediators to be linked to the formation of neovascular membranes was VEGF-A, which later emerged as the first therapeutic target. Along with additional angiogenic forms including VEGF-B and placental-like growth factor (PLGF), VEGF-A comes in a variety of isoforms. Ranibizumab, aflibercept, and bevacizumab are the three main intravitreal medications used to treat wet AMD. A recombinant monoclonal antibody fragment called ranibizumab is effective against all VEGF-A subtypes. Aflibercept, a fusion protein of the VEGF-trap and VEGF-A, binds to both growth factors. Bevacizumab, a monoclonal antibody used systemically to treat colon cancer, works by binding to all VEGF-A isoforms. While the FDA has approved the first two medications for exudative AMD, the third is used off-label. Faricimab and brolucizumab are recent pharmaceuticals. 2019 saw the FDA's approval of brolucizumab, a humanized single-chain monoclonal antibody fragment with the ability to bind to all human VEGF-A isoforms. On the other hand, faricimab is a particular antibody that specifically targets VEGF-A and angiopoietin-2 (Ang-2). Inhibiting Ang-2 is useful in lowering inflammation and edema development because it contributes to vascular endothelial stability and inflammation. [116]

Moreover, in the management of AMD, there are supportive systems, such as visual rehabilitation: these are optical systems that enlarge images, allowing for partial improvement of visual acuity, especially for close-up vision. [117]

1.4.3 Venous Occlusions

According to the site of occlusion there are two types of venous occlusions (VO): central retinal vein occlusion (CRVO) and branch retinal vein occlusion (BRVO) (superior, inferior, temporal, nasal). The two other categories of central retinal vein occlusions are non-ischemic and ischemic. [118]

1.4.3.1 Epidemiology

The worldwide prevalence of VO is estimated to be 0.4%, with equal distribution in both sexes and an increased risk with advanced age. [119]

1.4.3.2 Etiology and Risk Factors

The main risk factors are age, cardiovascular risk factors, arterial hypertension, diabetes mellitus, dyslipidemia, inflammatory conditions such as systemic lupus erythematosus, and coagulation disorders. [120-122]

1.4.3.3 Pathogenesis

In the retinal regions where arteries and veins cross, the adventitial layer is common. This implies that if the artery thickens, the vein, which has a thinner wall, is compressed. This occurs in the phenomenon of arteriosclerosis, where the arterial wall becomes thicker and consequently, at the crossroads, the adventitial layer cannot dilate, resulting in vein compression. Arteriovenous crossings are common in conditions such as arterial hypertension or diabetes. [123]

There are several factors that lead to venous thrombosis and subsequent retinal occlusion:

1. When the arteriolar/retinal artery thickens, the venule/retinal vein is compressed at the arteriovenous junction, resulting in turbulent flow and endothelial cell loss.
2. Wall alteration: some conditions that lead to loss of endothelium or pericytes result in platelet aggregation and thrombus formation.

3. Blood component pathologies: hypercoagulability, hyperaggregability, etc.
4. Slowing of blood velocity (often linked to decreased driving force in venous forms: if arterial supply is slowed, venous blood will also have reduced velocity).

Thrombosis leads to increased pressure upstream of the obstruction, resulting in circulatory slowdown with consequent retinal ischemia, wall damage with increased permeability, and rupture of capillaries. This leads to the formation of edema, hemorrhages, and compensatory circulation to bypass the occlusion itself. [124]

1.4.3.4 Clinical Presentation

Symptoms vary based on the location of the thrombosis. Typically, patients report sudden, painless visual decline, visual field constriction, and sudden haziness due to macular edema and hemorrhages. Occlusion can also be asymptomatic if a peripheral venous branch is involved. Macular edema leads to photoreceptor displacement, causing metamorphopsia – distorted vision due to intraretinal fluid. [125]

Fundus examination reveals:

- Dilation and tortuosity of veins in the affected segment.
- Flame, dot-like, or blot-shaped hemorrhages in the retinal area drained by the affected branch.
- Cotton-wool spots: soft, poorly defined margin exudates are an expression of ischemia since in some area's capillaries close, blood flow stops, leading to ischemic damage and formation of such exudates.
- Intraretinal edema: often not easily visible, requiring instrumental investigations like OCT.
- Collateral vessels: can form after several weeks in hypoperfused areas. They are a favorable prognostic factor as they spontaneously resolve the occlusion. After occlusion, the thrombus is remodeled, and there's some recovery of circulation patency. This initially occurs slowly, but there can be spontaneous bypass of the occlusion zone: new vessels form, connecting both sides of the occluded vein (upstream and downstream). These are neoformed but non-pathological vessels, unlike those resulting from ischemia.

- Retinal neovascularization: develops in 8% of eyes affected by retinal venous branch occlusion within 3 years; typically appearing 6-12 months after the event. Like diabetic retinopathy, neovascularization forms due to ischemia, leading to angiogenic factor production.
- Iris Neovascularization (Iris Rubeosis) and Neovascular Glaucoma: more common in central occlusions compared to branch occlusions. When VEGF is produced in large amount, it can reach the anterior segment and promote neovascularization at this level. In summary, a branch occlusion has the possibility to restore good circulation after the event, neovascularization occurs in few cases, and iris neovascularization occurs in very few cases.
- Chronic Macular Edema: It is the most common cause of long-term poor visual acuity.
- Tractional Retinal Detachment

1.4.3.5 Treatment

- *Laser treatment*: in the case of neovascularization development (since VEGF is produced by ischemic retinal areas), ischemic retinal areas need to be photocoagulated. Peripheral sectoral retinal photocoagulation in ischemic areas is indicated in the development of retinal and iris neovascularization or neovascular glaucoma.
- *Intravitreal therapy*: post-occlusion macular edema treatment is based on two molecules injected into the vitreous to reduce macular edema. These include slow-release steroids, particularly indicated in venous occlusions initially, and anti-VEGF agents secondarily. These treatments are often combined with laser therapy.
- *Macular microencapsulated laser*: used in macular edema treatment, with or without anti-VEGF therapy; less frequently used than intravitreal injections. [126, 127]

2 STUDY OBJECTIVE

The objective of the study was to create DL models capable of identifying key signs of retinal pathologies in fovea-centered OCT images. The models also aim to identify multiple retinal signs present in the same OCT scan.

3 MATERIALS AND METHODS

Patients were enrolled at the University Eye Clinic of Trieste. Every participant in this study gave their informed consent for the use of their data. The retrospective study was approved by the Ethics Committee with protocol number 17094/2022.

3.1 Data collection

Retrospective analysis was performed on fully anonymized OCT scans that used an A-line scanning procedure with a length of 9.0 mm. The Spectralis OCT device (Heidelberg Engineering, Heidelberg, Germany) was used to take these images. It uses an 815 nm laser source with an image size of 768x496 pixels.

The fovea was the focal point of both the horizontal and vertical line scans used in the study. These scans were taken from people who were both healthy and who had a variety of retinal disorders. Data was gathered for the study between January 2017 and September 2022, and participants' ages varied from 18 to 95.

ERM, Intraretinal Fluid (IF), Subretinal Fluid (SF), Drusen (D), MNV, Vitreomacular Adhesion (VMA), MH, and BS were required as inclusion criteria for the pathological group. Healthy group had normal OCT scans and showed no aberrant retinal signs. Images with a Spectralis Quality value below 23 were deemed to be of poor quality, and they were thus omitted from the research.

3.2 Image Labeling and Preprocessing

Two experienced retinal experts (LI, DM) examined and categorized each image in detail. Poor quality images, OCT scans not focused on the foveal region, and images for which the two experts could not concur were eliminated from the dataset.

Figure 2 presents illustrative OCT images for each of the recognized signs. Each image was cropped to the scan's center for standardization, giving it a 621x445 pixel size. They were then downsized to the VGG-16 convolutional neural networks algorithm's default input image size of 224x224 pixels. The bicubic interpolation method was used to achieve this resizing.

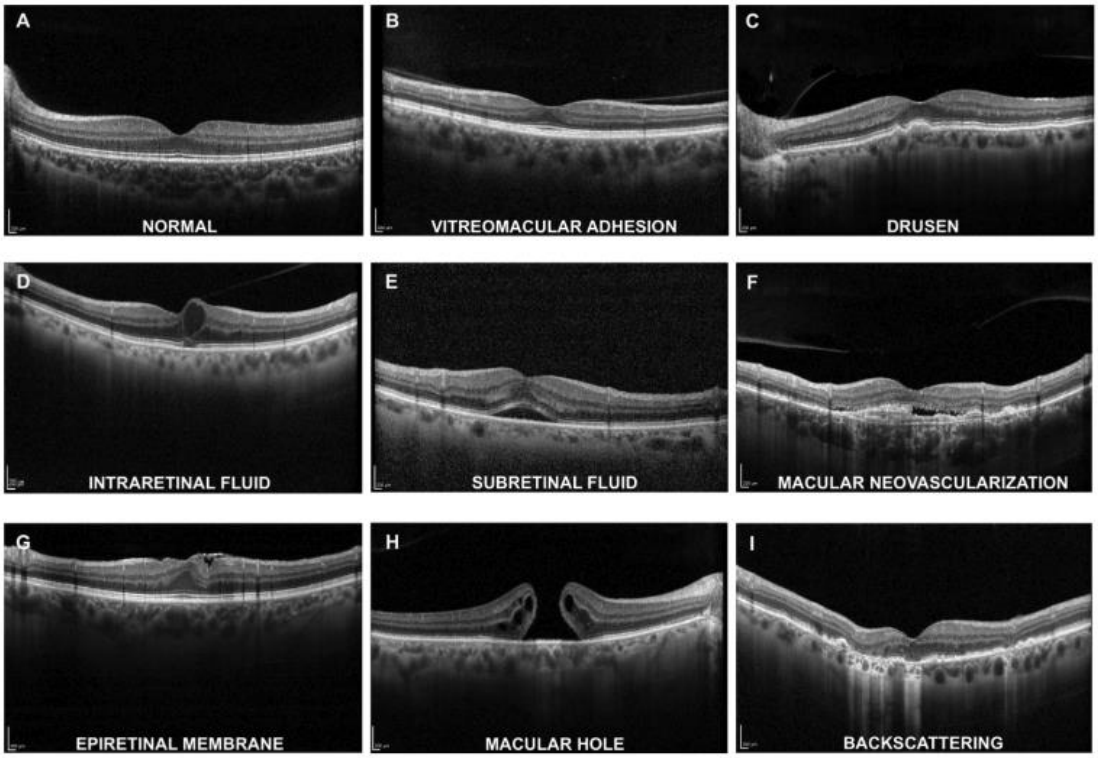

Figure 2

3.3 Datasets Population and Training Process

Nine different predictive binary models were created using preprocessing on the labeled images. The first model was trained to differentiate between healthy and pathological

eyes. The following eight models were then created to distinguish between distinct retinal degeneration signs. Images of both healthy eyes and eyes with at least one sign were used in the initial model. The remaining eight models each focused on images either having a certain sign or not having that sign. An equal number of images were considered for each group in every model to provide a balanced dataset. 10% of the images from healthy eyes and 10% of the images for each sign were randomly selected to create a test set. A 5-fold cross-validation was carried out using the remaining 90% of the images. The images with one or more aberrant signs are shown in table 1.

# of signs	BS	MNV	D	IF	SF	MH	ERM	VMA	Total images
1	212	96	1091	964	265	145	880	1733	5386
2	418	375	470	727	302	250	518	342	1701
3	257	245	95	296	130	80	156	70	443
4	83	88	37	88	52	12	27	33	105
5	15	15	5	11	13	2	6	8	15
Total	985	819	1698	2086	762	489	1587	2186	7650

Table 1

3.4 Modeling

We chose the VGG-16 model for this study from among the three widely used CNN architectures.

It is generally known that VGG is useful in medical diagnostic imaging. VGG consistently ranks among the top three CNN designs often used in the medical imaging area, according to an extended analysis spanning from 2012 to 2020. [128] Notably, VGG has proven to be incredibly accurate, obtaining an accuracy rate of almost 97.5% when making the diagnosis of Choroidal Neovascularization (CNV) using retinal OCT images. [129] A modified VGG16 architecture has also been presented for the categorization of diabetic retinopathy, outperforming state-of-the-art procedures in terms of accuracy while also optimizing the utilization of computational resources. [130] VGG16 has proven its adaptability in several fields outside of ophthalmology. It successfully classified breast cancer from mammography images, for example, earning a remarkable test score of 88%. [131] Moreover, VGG16 has demonstrated its ability in

the field of MRI-based brain tumor identification, claiming a remarkable accuracy rate of about 96.1%. Specifically, a UNet-VGG16 configuration with transfer learning was used to improve the segmentation of brain tumors in MRI images. [132] VGG16 was utilized as a pre-trained model in the field of breast histopathology image processing, enabling the extraction of complex characteristics to improve the categorization of breast cancer. [133] In addition, an improved iteration of the VGG16 model has been proposed for the classification of X-ray images connected to pneumonia demonstrating considerable performance improvements over other CNN. [134]

Nine binary classifiers were trained using the improved VGG-16 model. (Figure 3)

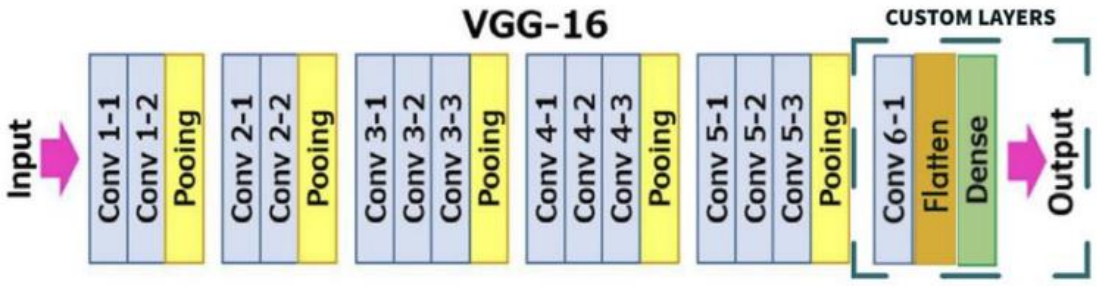

Figure 3

For each of the nine binary models, we employed transfer learning and fine-tuning approaches using the pre-trained VGG-16 model. As seen on the right side of Fig. 3, we updated the top layers of VGG-16 while leaving the earlier levels frozen to build the model. To ensure compatibility with dense layers that need 1D vectors as input, we included a sigmoid dense layer for classification and included a flattened layer to transform data from 3D tensors into one-dimensional arrays. Taking use of the patterns discovered in the previous convolutional layers, these further layers were trained using the Adaptive Moment Estimation Algorithm (ADAM) with a very low learning rate of 0.0001. [135]

This method allowed the detection of retinal defects even without retraining our VGG-16 model with our images. We used common data augmentation methods to resize and improve the images before training each model. We then started the training process by feeding the model batches of 32 of these images. There were two phases to the training

procedure. We used transfer learning in the first stage while keeping the convolutional layers frozen. In the second phase, we used the early stopping technique to halt training if the accuracy on the validation set did not increase after eight iterations.

Maximum 70 epochs were used in our training routine for each model, with a batch size of 32 elements being used consistently. The training was split into two parts, with the transfer learning phase receiving 40 epochs and the fine-tuning phase receiving the remaining 30 epochs. The choice of the maximum epoch count was decided using empirical data and taking the model's convergence trends into account. To continually evaluate each model's correctness on the validation datasets at each epoch, we adopted the early stopping technique. If no more performance enhancements were seen, the training procedure was immediately ended. After training, we selected the model that performed best on the validation set and tested it on the test sets.

We used a computer with a Ryzen 7 2700 CPU, an NVIDIA RTX 3070ti graphics card, and 16 GB of DDR4 RAM for the training procedure. For the training process, we used Python 3.10 and Keras, a high-level Tensorflow 2 API.

3.5 Evaluation metrics

We tested the model's performance by measuring accuracy, sensitivity, specificity, and the area under the ROC curve (AUC). We made use of confusion matrices to better explain misclassifications. To assess the consistency between the model's predictions and the actual labelling of the variables, we also computed Cohen's Kappa indices. The scikit-learn Python library was used for all these investigations.[136]

3.6 Model visualization (GRAD-CAM)

To get insight into the predictions, we employed the Gradient-weighted class activation mapping (Grad-CAM heatmap) technique for each CNN model. Grad-CAMs were utilized to determine the regions that had the most effect on the model's judgements just before the VGG16's final completely connected layer. We were able to visually locate the important characteristics or areas of interest in the input data that had a substantial impact on the model's judgement by creating heatmaps. This method helped to clarify

the reasoning behind the predictions made by the model. Grad-CAM heatmap samples are shown in Figure 4.

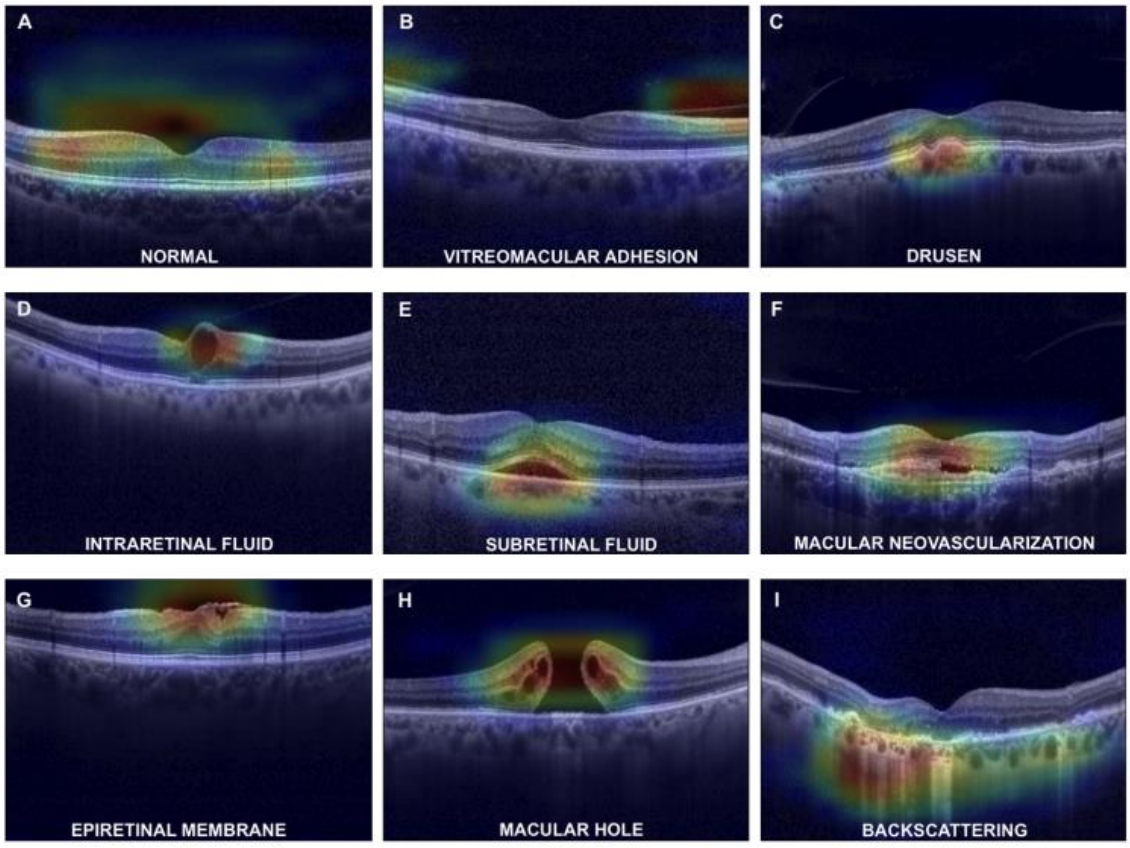

Figure 4

4 RESULTS

We included a total of 21,500 OCT scans from 11,245 individuals (5,258 men and 5,987 women), with an average age of 71.2 ± 16.5. The images were chosen randomly from Heidelberg Spectralis OCT database. After this first selection, 10,770 images were included tin the study. Of them, 7,650 were classified as pathological, whereas 3,120 were categorised as normal. Images that had several signs were tallied more than once. Thus, a total of 10,612 images showing one or more signs were included in the study, including 1,587 images with ERM, 2,086 with IF, 762 with SF, 1,698 with D, 819 with MNV, 2,186 with VMA, 489 with MH, and 985 with BS.

Nine distinct CNN models were developed and trained to distinguish between normal and pathological images. Additionally, these models were tasked with differentiating between various pathological signs. Figure 5 illustrates a typical progression where the accuracy metric consistently improves while the loss metric decreases during the training phases.

Figure 5

For the test and validation sets, we generated nine confusion matrices. The results are displayed in Tables 2 and 3. In these matrices, columns represent examples in the expected classes, while rows represent occurrences in the actual classes.

	HEALTHY	PATHOLOGICAL
HEALTHY	560	2
PATHOLOGICAL	8	553

	ERM	O.S.
ERM	441	11
O.S.	16	445

	IF	O.S.
IF	350	7
O.S.	3	353

	SF	O.S.
SF	118	8
O.S.	1	118

	D	O.S.
D	281	12
O.S.	11	281

	MNV	O.S.
MNV	107	9
O.S.	3	107

	VMA	O.S.
VMA	359	1
O.S.	6	354

	MH	O.S.
MH	85	3
O.S.	1	87

	BS	O.S.
BS	142	8
O.S.	14	148

Table 2

	HEALTHY	PATHOLOGICAL
HEALTHY	309	3
PATHOLOGICAL	6	306

	ERM	O.S.
ERM	249	4
O.S.	5	248

	IF	O.S.
IF	193	5
O.S.	0	197

	SF	O.S.
SF	68	2
O.S.	1	69

	D	O.S.
D	154	8
O.S.	10	152

	MNV	O.S.
MNV	58	6
O.S.	3	61

	VMA	O.S.
VMA	199	0
O.S.	3	197

	MH	O.S.
MH	46	2
O.S.	0	48

	BS	O.S.
BS	79	2
O.S.	0	83

Table 3

For each of the nine CNN models, the accuracy, sensitivity, specificity, kappa value, and AUC are shown in Tables 4 and 5, individually computed for the test and validation sets.

	Accuracy	Sensitivity	Specificity	Kappa	AUC
Healthy	0.99	1.00	0.99	0.98	0.99
ERM	0.97	0.96	0.98	0.94	0.97
IF	0.99	0.98	0.99	0.97	0.99
SF	0.96	0.94	0.99	0.93	0.96
D	0.96	0.96	0.96	0.92	0.96
MNV	0.95	0.92	0.97	0.90	0.95
VMA	0.99	1.00	0.98	0.98	0.99
MH	0.98	0.96	0.99	0.95	0.98
BS	0.93	0.91	0.95	0.86	0.93

Table 4

	Accuracy	Sensitivity	Specificity	Kappa	AUC
Healthy	0.99	0.99	0.98	0.97	0.99
ERM	0.98	0.98	0.98	0.96	0.98
IF	0.99	0.97	1.00	0.97	0.99
SF	0.98	0.97	0.99	0.96	0.98
D	0.94	0.95	0.94	0.89	0.94
MNV	0.93	0.91	0.95	0.86	0.93
VMA	0.99	1.00	0.98	0.98	0.99
MH	0.98	0.96	1.00	0.96	0.98
BS	0.94	0.92	0.96	0.88	0.94

Table 5

Figure 4 shows heatmaps for each pathological signs, which are useful for identifying and locating them as indicated by the algorithm. The Grad-CAM heatmaps example in Figure 6 illustrates how the system exhibited its capacity to recognize several signs inside a single OCT image. Figure 7 illustrates instances in which the CNNs produced inaccurate heatmaps.

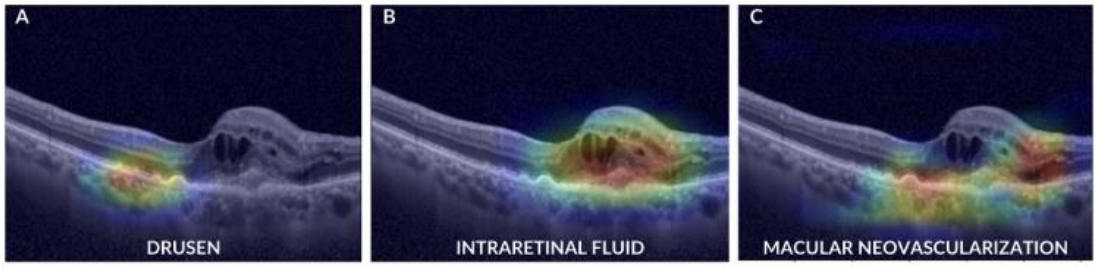

Figure 6

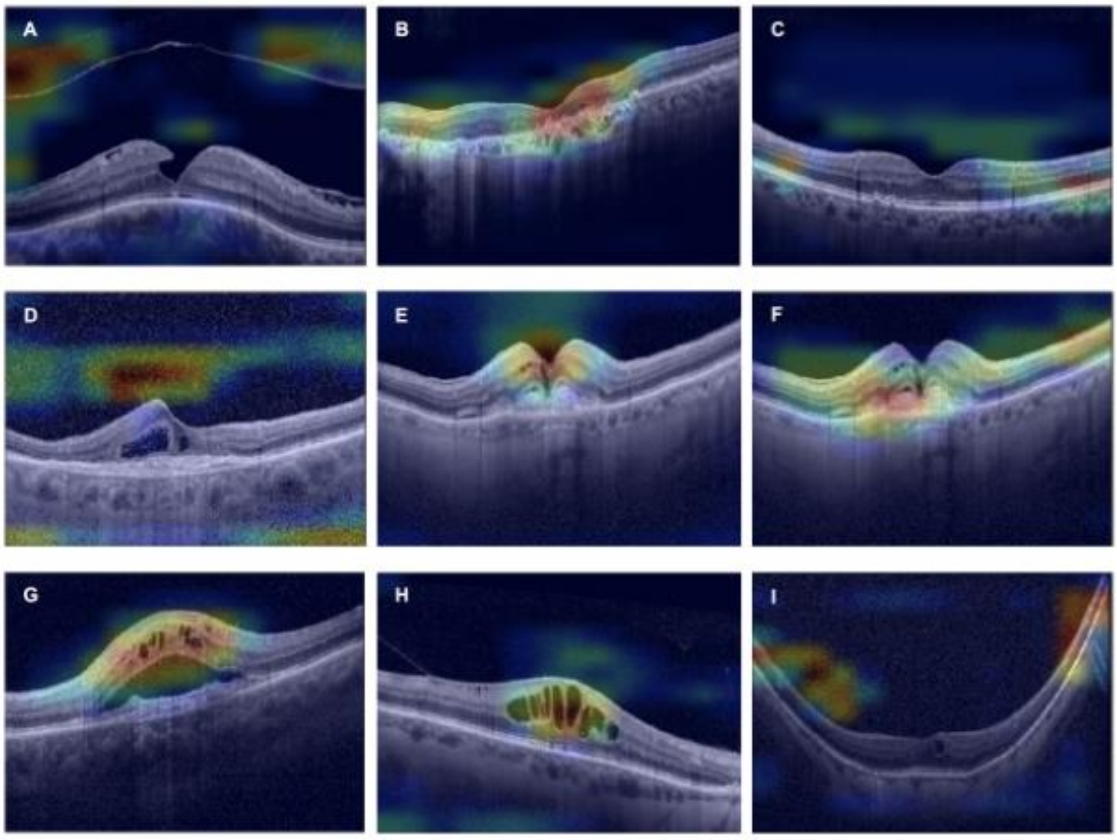

Figure 7

5 DISCUSSION

OCT is now a crucial diagnostic technique for several retinal diseases, including MH, ERM, AMD, and DR. Additional diagnostic techniques like fluorescein angiography and fundus images are used in conjunction. [137-141]

Using OCT, several studies have investigated the use of DL algorithms to identify diabetic retinopathy (DR) and diabetic macular edema. [142, 143-145] The exceptional area under the curve (AUC) of 0.958, 100% sensitivity, and 91.1% specificity that Ting's training of a DL system to recognize DR produced is only one example of the outstanding results she was able to obtain. [142] A DL method for automated macular edema segmentation was developed in 2017 by Lee and colleagues, who outperformed retina specialists in terms of performance. [146] Using a dataset of 62,489 OCT images, Kermany created a CNN capable of differentiating between normal cases and DR, attaining outstanding accuracy of 98.2%, a sensitivity of 96.8%, and a specificity of 99.6%. [147] In 2017, Schlegl and colleagues created an automated approach for detecting and quantifying intraretinal cystoid fluid, reaching an AUC of 0.94. [40] With an AUC of 0.98, a sensitivity of 96.8%, and a specificity of 87.0%, the CNN developed by Abràmoff et al. performed well in identifying DR on OCT images. [148]

Burlina and colleagues' AI model shown remarkable skills in identifying AMD from OCT images, attaining notable accuracy ranging between around 92% and 95% across distinct groups. [149] Similar results were obtained by Ting and his colleagues, who created a DL system capable of identifying AMD in a multiethnic sample of diabetic patients. This system produced outstanding results, including an AUC of 0.93, a sensitivity of 93.2%, and a specificity of 88.7%. [142] The accuracy, sensitivity, and specificity of Kermany and colleagues' excellent diagnostic performance for AMD utilizing OCT images were 96.6%, 97.8%, and 97.4% [147]. Additionally, CNNs were trained by other authors to recognize certain biomarkers linked to the prognosis and development of AMD [150–156].

According to Yanagihara and colleagues [157], the application of much research is still limited in clinical practice in actual hospital settings. The restricted interpretability of DL models and the use of non-standard datasets are two of the many difficulties encountered. This situation frequently requires that every hospital create its own dataset.

To differentiate between pathological and normal OCT images, all the aforementioned research used binary classification approaches. By basing diagnoses on specific OCT images, they all functioned inside a black-box framework. Clinical diagnoses, however, rely on the detection of anomalies throughout a collection of OCT images acquired from the same patient, as a single scan could not include all the necessary data. The classification of retinal abnormality signs rather than the disorders themselves is one possible strategy for overcoming this difficulty. It is important to note that few research have documented the identification of such signs. Son and colleagues created a DL model that uses macula-centered fundus images to efficiently identify 15 aberrant retinal signs and offer diagnosis for 8 main eye diseases. To clarify the diagnostic logic used by the system and throw light on the significance of each anomalous result to its prediction, they developed the idea of counterfactual attribution ratio (CAR). CAR enables interactive changes, quantitative and qualitative interpretations, and confirmation of the model's ability to recognize observations and disorders in a way like ophthalmologists. [158] A DL system that can distinguish between normal images and those showing cystoid macular edema, serous macular detachment, ERM and MH was proposed by Lu and colleagues in a research. The system achieved an accuracy of 97%, 84%, 94%, 96%, and 98%, respectively. [159] Additionally, with 97% accuracy, 93% sensitivity, and 98% specificity, Rajagopalan et al. diagnosed CNV, D, and diabetic macular edema (DME). [160] Kurmann used a machine learning method in a separate work to recognize a variety of conditions in OCT B-scan images. These conditions included geographic atrophy (GA), outer retinal atrophy (ORA), SRF, IRF, intraretinal cysts (IRC), hyperreflective foci (HF), D, reticular pseudodrusen (RPD), ERM, and fibrovascular pigment epithelial detachment (FPED). Their DL system produced excellent results after being trained on a dataset made up of 23,030 OCT images. [161]

Like Kurmann's method, we trained our DL models using simple datasets that were easily acquired from a single hospital environment. These models were created with the particular purpose of detecting different retinal abnormalities in a single OCT image. They mimic the logical method used by ophthalmologists to diagnose ocular disorders by identifying specific abnormality signs rather than depending exclusively on the results produced by a black-box DL model. Our goal was to closely resemble the clinical process, in which doctors use a variety of images to evaluate the existence of all nine signs. By reviewing the classifier output, which contains class probabilities, and examining the heatmaps, we wanted to acquire a thorough understanding of the sign

recognition procedure. Additionally, this method lessens the overall number of images generally required to distinguish between different diseases. The CNN architecture used by VGG-16 is quite simple and consists of a series of convolutional layers, followed by max-pooling and fully linked layers. Because of its simplicity, the VGG-16 model has fewer parameters than ResNet and Inception, which have more complex designs that include skip connections, residual blocks, and inception modules and can thus capture more complex information.

CNN was successfully used by Lee et al. to distinguish between normal OCT images and those from AMD patients.[162] They gathered a sizable collection of several OCT images for their investigation from both healthy volunteers and AMD patients. Out of these, 20,163 images were set aside for validation purposes and 80,839 images were chosen for training a CNN model. AUCs of 92.78%, 93.83%, and 97.45% were obtained from the image level, macular level, and patient level ROC curves, respectively. In a work by Choi et al., they developed three CNNs and trained and validated them to classify OCT images into three categories: normal, high myopia, and various retinal disorders. [163] Their strategy includes building models for image categorization using three different architectural backbones: VGG-16, ResNet-50, and Inception-v3. The effectiveness of these models was evaluated, and the best AUCs were obtained for the following models: ResNet-50, 99.9% for VGG-16, and 96.1% for Inception-v3.

In contrast to earlier research, our models were able to obtain a noticeably high degree of accuracy on both the training and test datasets, ranging from 93% to 99%, while using a more straightforward architecture. This precision applies to the detection of eight disease signs as well as healthy retinas. The robustness of our models is suggested by their consistent performance on both the validation and test datasets, which shows that they did not overfit during training and were good at capturing the underlying patterns associated with retinal abnormality signs. Therefore, as shown by the compelling findings, these models showed the ability to successfully categories such signs, whether single or multiple, in a single OCT image.

We understand that VGG16 is not the most advanced architecture and might not achieve the highest levels of accuracy. However, it has proven that it can obtain clinically applicable findings when identifying signs of retinal degeneration.

The time it took to classify an image in our unique scenario with our computer was about 2.2 seconds. It's important to emphasize that, while getting extremely high accuracy rates (e.g., close to 100%) may not be feasible for some medical imaging activities, achieving accuracy levels that have therapeutic value should be the main goal. [164,165]

The specific medical goal, potential effects on patient care, and special use-case situation can all have an impact on how variable these values are. [166]

Notably, our approach enables ophthalmologists to evaluate every OCT image independently, acknowledging that not all signs may be seen in every scan. Additionally, because the system can identify distinct signs rather than being restricted to just one type of retinal pathology, it might serve as a diagnostic aid for a wider range of disorders that show different combinations of these signs. It's important to note that the classification of specific signs may be considered as a drawback because it still requires ophthalmologist involvement to diagnose a condition, which is frequently required in automated screening systems.

6 CONCLUSIONS

The effectiveness of adding more recent DL architectures into the diagnostic workflow should be improved further by examining the practicality of doing so and assessing their performance. Finally, our findings show that DL models have the potential to enhance ocular pathology diagnosis and clinical decision-making.

7 REFERENCES

[1] K. H. Yu, A. L. Beam, and I. S. Kohane, "Artificial intelligence in healthcare," *Nature Biomedical Engineering*, vol. 2, no. 10. Nature Publishing Group, pp. 719–731, Oct. 01, 2018. doi: 10.1038/s41551-018-0305-z.

[2] Y. Mintz and R. Brodie, "Introduction to artificial intelligence in medicine," *Minimally Invasive Therapy and Allied Technologies*, vol. 28, no. 2, pp. 73–81, Mar. 2019, doi: 10.1080/13645706.2019.1575882.

[3] M. D. Abràmoff *et al.*, "Improved automated detection of diabetic retinopathy on a publicly available dataset through integration of deep learning," *Invest Ophthalmol Vis Sci*, vol. 57, no. 13, pp. 5200–5206, Oct. 2016, doi: 10.1167/iovs.16-19964.

[4] F. Li *et al.*, "Automatic differentiation of Glaucoma visual field from non-glaucoma visual filed using deep convolutional neural network," *BMC Med Imaging*, vol. 18, no. 1, p. 35, Dec. 2018, doi: 10.1186/s12880-018-0273-5.

[5] F. Grassmann *et al.*, "A Deep Learning Algorithm for Prediction of Age-Related Eye Disease Study Severity Scale for Age-Related Macular Degeneration from Color Fundus Photography," *Ophthalmology*, vol. 125, no. 9, pp. 1410–1420, Sep. 2018, doi: 10.1016/j.ophtha.2018.02.037.

[6] P. M. Burlina, N. Joshi, M. Pekala, K. D. Pacheco, D. E. Freund, and N. M. Bressler, "Automated grading of age-related macular degeneration from color fundus images using deep convolutional neural networks," *JAMA Ophthalmol*, vol. 135, no. 11, pp. 1170–1176, Nov. 2017, doi: 10.1001/jamaophthalmol.2017.3782.

[7] D. S. J. Ting *et al.*, "Artificial intelligence for anterior segment diseases: Emerging applications in ophthalmology," *British Journal of Ophthalmology*, vol. 105, no. 2. BMJ Publishing Group, pp. 158–168, Feb. 01, 2021. doi: 10.1136/bjophthalmol-2019-315651.

[8] M. K. Smolek and S. D. : Klyce, "Current Keratoconus Detection Methods Compared With a Neural Network Approach," *Investigative ohthalmology & visual science*, 1997.

[9] M. A. Valdés-Mas *et al.*, "A new approach based on Machine Learning for predicting corneal curvature (K1) and astigmatism in patients with keratoconus after intracorneal ring implantation," *Comput Methods Programs Biomed*, vol. 116, no. 1, pp. 39–47, Aug. 2014, doi: 10.1016/j.cmpb.2014.04.003.

[10] T. Cui *et al.*, "Applying Machine Learning Techniques in Nomogram Prediction and Analysis for SMILE Treatment," *Am J Ophthalmol*, vol. 210, pp. 71–77, Feb. 2020, doi: 10.1016/j.ajo.2019.10.015.

[11] A. Achiron *et al.*, "Predicting Refractive Surgery Outcome: Machine Learning Approach With Big Data," *Journal of Refractive Surgery*, vol. 33, no. 9, pp. 592–597, Sep. 2017, doi: 10.3928/1081597X-20170616-03.

[12] L. Ung, P. J. M. Bispo, S. S. Shanbhag, M. S. Gilmore, and J. Chodosh, "The persistent dilemma of microbial keratitis: Global burden, diagnosis, and antimicrobial resistance," *Surv Ophthalmol*, vol. 64, no. 3, pp. 255–271, May 2019, doi: 10.1016/j.survophthal.2018.12.003.

[13] Jagjit S. S., Arun K. J., Sanjay K., Siddharth V., Sidharath P., and Simardeep S., "Neural network approach to classify infective keratitis," *Curr Eye Res*, 2003.

[14] J. S. Saini, A. K. Jain, S. Kumar, S. Vikal, S. Pankaj, and S. Singh, "Neural network approach to classify infective keratitis," *Curr Eye Res*, vol. 27, no. 2, pp. 111–116, Jan. 2003, doi: 10.1076/ceyr.27.2.111.15949.

[15] T. Hayashi *et al.*, "A Deep Learning Approach in Rebubbling after Descemet's Membrane Endothelial Keratoplasty," *Eye Contact Lens*, vol. 46, no. 2, pp. 121–126, Mar. 2020, doi: 10.1097/ICL.0000000000000634.

[16] W. M. D. Wan Zaki, M. Mat Daud, S. R. Abdani, A. Hussain, and H. A. Mutalib, "Automated pterygium detection method of anterior segment photographed images," *Comput Methods Programs Biomed*, vol. 154, pp. 71–78, Feb. 2018, doi: 10.1016/j.cmpb.2017.10.026.

[17] Y. P. Lopez and L. R. Aguilera, "Automatic Classification of Pterygium-Non Pterygium Images Using Deep Learning," 2019, pp. 391–400. doi: 10.1007/978-3-030-32040-9_40.

[18] M. A. Zulkifley, S. R. Abdani, and N. H. Zulkifley, "Pterygium-Net: a deep learning approach to pterygium detection and localization," *Multimed Tools Appl*, vol. 78, no. 24, pp. 34563–34584, Dec. 2019, doi: 10.1007/s11042-019-08130-x.

[19] S. R. Flaxman *et al.*, "Global causes of blindness and distance vision impairment 1990–2020: a systematic review and meta-analysis," *Lancet Glob Health*, vol. 5, no. 12, pp. e1221–e1234, Dec. 2017, doi: 10.1016/S2214-109X(17)30393-5.

[20] W. Wang *et al.*, "Cataract Surgical Rate and Socioeconomics: A Global Study," *Investigative Opthalmology & Visual Science*, vol. 57, no. 14, p. 5872, Jan. 2017, doi: 10.1167/iovs.16-19894.

[21] L. T. Chylack, "The Lens Opacities Classification System III," *Archives of Ophthalmology*, vol. 111, no. 6, p. 831, Jun. 1993, doi: 10.1001/archopht.1993.01090060119035.

[22] J. Panchapakesan, R. G. Cumming, and P. Mitchell, "Reproducibility of the Wisconsin cataract grading system in the Blue Mountains Eye Study," *Ophthalmic Epidemiol*, vol. 4, no. 3, pp. 119–126, Jan. 1997, doi: 10.3109/09286589709115719.

[23] D. S. J. Ting, M. Ang, J. S. Mehta, and D. S. W. Ting, "Artificial intelligence-assisted telemedicine platform for cataract screening and management: a potential model of care for global eye health," *British Journal of Ophthalmology*, vol. 103, no. 11, pp. 1537–1538, Nov. 2019, doi: 10.1136/bjophthalmol-2019-315025.

[24] X. Wu *et al.*, "Universal artificial intelligence platform for collaborative management of cataracts," *British Journal of Ophthalmology*, vol. 103, no. 11, pp. 1553–1560, Nov. 2019, doi: 10.1136/bjophthalmol-2019-314729.

[25] M. Sramka, M. Slovak, J. Tuckova, and P. Stodulka, "Improving clinical refractive results of cataract surgery by machine learning," *PeerJ*, vol. 7, p. e7202, Jul. 2019, doi: 10.7717/peerj.7202.

[26] R. Koprowski, M. Lanza, and C. Irregolare, "Corneal power evaluation after myopic corneal refractive surgery using artificial neural networks," *Biomed Eng Online*, vol. 15, no. 1, p. 121, Dec. 2016, doi: 10.1186/s12938-016-0243-5.

[27] M. R. Razeghinejad and J. S. Myers, "Contemporary approach to the diagnosis and management of primary angle-closure disease," *Surv Ophthalmol*, vol. 63, no. 6, pp. 754–768, Nov. 2018, doi: 10.1016/j.survophthal.2018.05.001.

[28] J. Benitez-del-Castillo, A. Nowrouzi, M. Rodriguez-Calzadilla, I. Mota-Chozas, and M. D. Pinazo-Duran, "Detection of occludable angle with anterior segment optical coherence tomography and

Pentacam as non-contact screening methods," *Int Ophthalmol*, vol. 42, no. 7, pp. 2093–2105, Jul. 2022, doi: 10.1007/s10792-021-02208-y.

[29] N. Porporato, M. Baskaran, and T. Aung, "Role of anterior segment optical coherence tomography in angle-closure disease: a review," *Clin Exp Ophthalmol*, vol. 46, no. 2, pp. 147–157, Mar. 2018, doi: 10.1111/ceo.13120.

[30] W. P. Nolan *et al.*, "Detection of Primary Angle Closure Using Anterior Segment Optical Coherence Tomography in Asian Eyes," *Ophthalmology*, vol. 114, no. 1, pp. 33–39, Jan. 2007, doi: 10.1016/j.ophtha.2006.05.073.

[31] M. E. Nongpiur *et al.*, "Classification Algorithms Based on Anterior Segment Optical Coherence Tomography Measurements for Detection of Angle Closure," *Ophthalmology*, vol. 120, no. 1, pp. 48–54, Jan. 2013, doi: 10.1016/j.ophtha.2012.07.005.

[32] S. I. Niwas *et al.*, "Automated anterior segment OCT image analysis for Angle Closure Glaucoma mechanisms classification," *Comput Methods Programs Biomed*, vol. 130, pp. 65–75, Jul. 2016, doi: 10.1016/j.cmpb.2016.03.018.

[33] B. Y. Xu, M. Chiang, S. Chaudhary, S. Kulkarni, A. A. Pardeshi, and R. Varma, "Deep Learning Classifiers for Automated Detection of Gonioscopic Angle Closure Based on Anterior Segment OCT Images," *Am J Ophthalmol*, vol. 208, pp. 273–280, Dec. 2019, doi: 10.1016/j.ajo.2019.08.004.

[34] H. Fu *et al.*, "A Deep Learning System for Automated Angle-Closure Detection in Anterior Segment Optical Coherence Tomography Images," *Am J Ophthalmol*, vol. 203, pp. 37–45, Jul. 2019, doi: 10.1016/j.ajo.2019.02.028.

[35] X. L. Du, W. B. Li, and B. J. Hu, "Application of artificial intelligence in ophthalmology," *International Journal of Ophthalmology*, vol. 11, no. 9. International Journal of Ophthalmology (c/o Editorial Office), pp. 1555–1561, 2018. doi: 10.18240/ijo.2018.09.21.

[36] G. A. Saleh *et al.*, "The Role of Medical Image Modalities and AI in the Early Detection, Diagnosis and Grading of Retinal Diseases: A Survey," *Bioengineering*, vol. 9, no. 8. MDPI, Aug. 01, 2022. doi: 10.3390/bioengineering9080366.

[37] M. Lin, G. Bao, X. Sang, and Y. Wu, "Recent Advanced Deep Learning Architectures for Retinal Fluid Segmentation on Optical Coherence Tomography Images," *Sensors*, vol. 22, no. 8. MDPI, Apr. 02, 2022. doi: 10.3390/s22083055.

[38] D. S. W. Ting *et al.*, "Development and validation of a deep learning system for diabetic retinopathy and related eye diseases using retinal images from multiethnic populations with diabetes," *JAMA - Journal of the American Medical Association*, vol. 318, no. 22, pp. 2211–2223, Dec. 2017, doi: 10.1001/jama.2017.18152.

[39] D. S. W. Ting *et al.*, "Artificial intelligence and deep learning in ophthalmology," *British Journal of Ophthalmology*, vol. 103, no. 2. BMJ Publishing Group, pp. 167–175, Feb. 01, 2019. doi: 10.1136/bjophthalmol-2018-313173.

[40] D. T. Hogarty, D. A. Mackey, and A. W. Hewitt, "Current state and future prospects of artificial intelligence in ophthalmology: a review," *Clinical and Experimental Ophthalmology*, vol. 47, no. 1. Blackwell Publishing, pp. 128–139, Jan. 01, 2019. doi: 10.1111/ceo.13381.

[41] A. G. Podoleanu, "Optical coherence tomography," *J Microsc*, vol. 247, no. 3, pp. 209–219, Sep. 2012, doi: 10.1111/j.1365-2818.2012.03619.x.

[42] S. Aumann, S. Donner, J. Fischer, and F. Müller, "Optical Coherence Tomography (OCT): Principle and Technical Realization," in *High Resolution Imaging in Microscopy and Ophthalmology*, Springer International Publishing, 2019, pp. 59–85. doi: 10.1007/978-3-030-16638-0_3.

[43] W. DREXLER and J. FUJIMOTO, "State-of-the-art retinal optical coherence tomography," *Prog Retin Eye Res*, vol. 27, no. 1, pp. 45–88, Jan. 2008, doi: 10.1016/j.preteyeres.2007.07.005.

[44] T. J. Heesterbeek, L. Lorés- Motta, C. B. Hoyng, Y. T. E. Lechanteur, and A. I. den Hollander, "Risk factors for progression of age- related macular degeneration," *Ophthalmic and Physiological Optics*, vol. 40, no. 2, pp. 140–170, Mar. 2020, doi: 10.1111/opo.12675.

[45] A. A. Bergen *et al.*, "On the origin of proteins in human drusen: The meet, greet and stick hypothesis," *Prog Retin Eye Res*, vol. 70, pp. 55–84, May 2019, doi: 10.1016/j.preteyeres.2018.12.003.

[46] A. M. VanDenLangenberg and M. P. Carson, *Drusen Bodies*. 2023.

[47] D. Rajapakse *et al.*, "Amelotin is expressed in retinal pigment epithelium and localizes to hydroxyapatite deposits in dry age-related macular degeneration," *Translational Research*, vol. 219, pp. 45–62, May 2020, doi: 10.1016/j.trsl.2020.02.007.

[45] K. N. Khan *et al.*, "Differentiating drusen: Drusen and drusen-like appearances associated with ageing, age-related macular degeneration, inherited eye disease and other pathological processes," *Prog Retin Eye Res*, vol. 53, pp. 70–106, Jul. 2016, doi: 10.1016/j.preteyeres.2016.04.008.

[46] N. T. M. Saksens *et al.*, "Macular dystrophies mimicking age-related macular degeneration," *Prog Retin Eye Res*, vol. 39, pp. 23–57, Mar. 2014, doi: 10.1016/j.preteyeres.2013.11.001.

[47] Y. Zheng, J. Sahni, C. Campa, A. N. Stangos, A. Raj, and S. P. Harding, "Computerized assessment of intraretinal and subretinal fluid regions in spectral-domain optical coherence tomography images of the retina," *Am J Ophthalmol*, vol. 155, no. 2, 2013, doi: 10.1016/j.ajo.2012.07.030.

[48] J. Chen and L. Lee, "Clinical applications and new developments of optical coherence tomography: an evidence- based review," *Clin Exp Optom*, vol. 90, no. 5, pp. 317–335, Sep. 2007, doi: 10.1111/j.1444-0938.2007.00151.x.

[49] W. R. Green and D. J. Wilson, "Choroidal Neovascularization," *Ophthalmology*, vol. 93, no. 9, pp. 1169–1176, 1986, doi: 10.1016/S0161-6420(86)33609-1.

[50] N. M. Bressler, S. B. Bressler, and E. S. Gragoudas, "Clinical Characteristics of Choroidal Neovascular Membranes," *Archives of Ophthalmology*, vol. 105, no. 2, pp. 209–213, Feb. 1987, doi: 10.1001/archopht.1987.01060020063030.

[51] J. D. Gass, "Pathogenesis of disciform detachment of the neuroepithelium.," *Am J Ophthalmol*, vol. 63, no. 3, p. Suppl:1-139, Mar. 1967.

[52] M. L. Small, "Senile Macular Degeneration," *Archives of Ophthalmology*, vol. 94, no. 4, p. 601, Apr. 1976, doi: 10.1001/archopht.1976.03910030287008.

[53] R. F. Spaide *et al.*, "Consensus Nomenclature for Reporting Neovascular Age-Related Macular Degeneration Data," *Ophthalmology*, vol. 127, no. 5, pp. 616–636, May 2020, doi: 10.1016/j.ophtha.2019.11.004.

[54] S. Sivaprasad *et al.*, "Diagnostic Accuracy of Monitoring Tests of Fellow Eyes in Patients with Unilateral Neovascular Age-Related Macular Degeneration," *Ophthalmology*, vol. 128, no. 12, pp. 1736–1747, Dec. 2021, doi: 10.1016/j.ophtha.2021.07.025.

[55] D. V. Do *et al.*, “Detection of New-Onset Choroidal Neovascularization Using Optical Coherence Tomography,” *Ophthalmology*, vol. 119, no. 4, pp. 771–778, Apr. 2012, doi: 10.1016/j.ophtha.2011.10.019.

[56] M. L. Small, “Senile Macular Degeneration,” Archives of Ophthalmology, vol. 94, no. 4, p. 601, Apr. 1976, doi: 10.1001/archopht.1976.03910030287008.

[57] R. F. Spaide et al., “Consensus Nomenclature for Reporting Neovascular Age-Related Macular Degeneration Data,” Ophthalmology, vol. 127, no. 5, pp. 616–636, May 2020, doi: 10.1016/j.ophtha.2019.11.004.

[58] S. Sivaprasad et al., “Diagnostic Accuracy of Monitoring Tests of Fellow Eyes in Patients with Unilateral Neovascular Age-Related Macular Degeneration,” Ophthalmology, vol. 128, no. 12, pp. 1736–1747, Dec. 2021, doi: 10.1016/j.ophtha.2021.07.025.

[59] D. V. Do et al., “Detection of New-Onset Choroidal Neovascularization Using Optical Coherence Tomography,” Ophthalmology, vol. 119, no. 4, pp. 771–778, Apr. 2012, doi: 10.1016/j.ophtha.2011.10.019.

[60] P. A. Keane, P. J. Patel, S. Liakopoulos, F. M. Heussen, S. R. Sadda, and A. Tufail, “Evaluation of Age-related Macular Degeneration With Optical Coherence Tomography,” Survey of Ophthalmology, vol. 57, no. 5. pp. 389–414, Sep. 2012. doi: 10.1016/j.survophthal.2012.01.006.

[61] B. J. Lujan, A. Roorda, R. W. Knighton, and J. Carroll, “Revealing Henle’s Fiber Layer Using Spectral Domain Optical Coherence Tomography,” Investigative Opthalmology & Visual Science, vol. 52, no. 3, p. 1486, Mar. 2011, doi: 10.1167/iovs.10-5946.

[62] M. Brar et al., “Colour versus grey-scale display of images on high-resolution spectral OCT,” British Journal of Ophthalmology, vol. 93, no. 5, pp. 597–602, May 2009, doi: 10.1136/bjo.2008.146233.

[63] J. Ho et al., “Documentation of Intraretinal Retinal Pigment Epithelium Migration via High-Speed Ultrahigh-Resolution Optical Coherence Tomography,” Ophthalmology, vol. 118, no. 4, pp. 687–693, Apr. 2011, doi: 10.1016/j.ophtha.2010.08.010.

[64] U. E. K. Wolf-Schnurrbusch, V. Enzmann, C. K. Brinkmann, and S. Wolf, “Morphologic Changes in Patients with Geographic Atrophy Assessed with a Novel Spectral OCT–SLO Combination,” Investigative Opthalmology & Visual Science, vol. 49, no. 7, p. 3095, Jul. 2008, doi: 10.1167/iovs.07-1460.

[65] P. Mitchell, W. Smith, T. Chey, J. J. Wang, and A. Chang, “Prevalence and Associations of Epiretinal Membranes,” Ophthalmology, vol. 104, no. 6, pp. 1033–1040, Jun. 1997, doi: 10.1016/S0161-6420(97)30190-0.

[66] D. J. McCarty et al., “Prevalence and Associations of Epiretinal Membranes in the Visual Impairment Project,” Am J Ophthalmol, vol. 140, no. 2, pp. 288.e1-288.e8, Aug. 2005, doi: 10.1016/j.ajo.2005.03.032.

[67] M. Inoue and K. Kadonosono, “Macular diseases: Epiretinal membrane,” Dev Ophthalmol, vol. 54, pp. 159–163, 2014, doi: 10.1159/000360462.

[68] A. T. Fung, J. Galvin, and T. Tran, “Epiretinal membrane: A review,” Clinical and Experimental Ophthalmology, vol. 49, no. 3. John Wiley and Sons Inc, pp. 289–308, Apr. 01, 2021. doi: 10.1111/ceo.13914.

[69] Gass JDM, “Stereoscopic Atlas of Macular Disease,” 1987, pp. 693–695.

[70] J. P. Hubschman et al., “Optical coherence tomography-based consensus definition for lamellar macular hole,” British Journal of Ophthalmology, vol. 104, no. 12, pp. 1741–1747, Dec. 2020, doi: 10.1136/bjophthalmol-2019-315432.

[71] N. G. Congdon, “Important Causes of Visual Impairment in the World Today,” *JAMA*, vol. 290, no. 15, p. 2057, Oct. 2003, doi: 10.1001/jama.290.15.2057.

[72] V. S. E. Jeganathan, J. J. Wang, and T. Y. Wong, “Ocular Associations of Diabetes Other Than Diabetic Retinopathy,” *Diabetes Care*, vol. 31, no. 9, pp. 1905–1912, Sep. 2008, doi: 10.2337/dc08-0342.

[73] A. N. Kollias and M. W. Ulbig, “Diabetic Retinopathy,” *Dtsch Arztebl Int*, Feb. 2010, doi: 10.3238/arztebl.2010.0075.

[74] N. Cheung, S. Rogers, D. J. Couper, R. Klein, A. R. Sharrett, and T. Y. Wong, “Is Diabetic Retinopathy an Independent Risk Factor For Ischemic Stroke?,” *Stroke*, vol. 38, no. 2, pp. 398–401, Feb. 2007, doi: 10.1161/01.STR.0000254547.91276.50.

[75] N. Cheung, J. J. Wang, R. Klein, D. J. Couper, A. R. Sharrett, and T. Y. Wong, “Diabetic Retinopathy and the Risk of Coronary Heart Disease,” *Diabetes Care*, vol. 30, no. 7, pp. 1742–1746, Jul. 2007, doi: 10.2337/dc07-0264.

[76] N. Cheung *et al.*, “Diabetic Retinopathy and Risk of Heart Failure,” *J Am Coll Cardiol*, vol. 51, no. 16, pp. 1573–1578, Apr. 2008, doi: 10.1016/j.jacc.2007.11.076.

[77] N. Cheung and T. Y. Wong, “Diabetic retinopathy and systemic vascular complications,” *Prog Retin Eye Res*, vol. 27, no. 2, pp. 161–176, Mar. 2008, doi: 10.1016/j.preteyeres.2007.12.001.

[78] D. A. Antonetti, R. Klein, and T. W. Gardner, “Diabetic Retinopathy,” *New England Journal of Medicine*, vol. 366, no. 13, pp. 1227–1239, Mar. 2012, doi: 10.1056/NEJMra1005073.

[79] T. Oshitari, “The Pathogenesis and Therapeutic Approaches of Diabetic Neuropathy in the Retina,” *Int J Mol Sci*, vol. 22, no. 16, p. 9050, Aug. 2021, doi: 10.3390/ijms22169050.

[80] F. Bandello *et al.*, “Diabetic Macular Edema,” 2017, pp. 102–138. doi: 10.1159/000455277.

[81] “Grading diabetic retinopathy from stereoscopic color fundus photographs--an extension of the modified Airlie House classification. ETDRS report number 10. Early Treatment Diabetic Retinopathy Study Research Group.,” *Ophthalmology*, vol. 98, no. 5 Suppl, pp. 786–806, May 1991.

[82] C. P. Wilkinson *et al.*, “Proposed international clinical diabetic retinopathy and diabetic macular edema disease severity scales,” *Ophthalmology*, vol. 110, no. 9, pp. 1677–1682, Sep. 2003, doi: 10.1016/S0161-6420(03)00475-5.

[83] A. Witkin and D. Salz, “Imaging in diabetic retinopathy,” *Middle East Afr J Ophthalmol*, vol. 22, no. 2, p. 145, 2015, doi: 10.4103/0974-9233.151887.

[84] T. H. Rim, A. W. J. Teo, H. H. S. Yang, C. Y. Cheung, and T. Y. Wong, “Retinal Vascular Signs and Cerebrovascular Diseases,” *Journal of Neuro-Ophthalmology*, vol. 40, no. 1, pp. 44–59, Mar. 2020, doi: 10.1097/WNO.0000000000000888.

[85] A. Moreno, M. Lozano, and P. Salinas, “Diabetic retinopathy.,” *Nutr Hosp*, vol. 28 Suppl 2, pp. 53–6, Mar. 2013, doi: 10.3305/nh.2013.28.sup2.6714.

[86] U. V. Shukla and E. J. Kaufman, *Intraocular Hemorrhage*. 2023.

[87] D. E. Singer, “Screening for Diabetic Retinopathy,” *Ann Intern Med*, vol. 116, no. 8, p. 660, Apr. 1992, doi: 10.7326/0003-4819-116-8-660.

[88] “Intensive blood-glucose control with sulphonylureas or insulin compared with conventional treatment and risk of complications in patients with type 2 diabetes (UKPDS 33). UK Prospective Diabetes Study (UKPDS) Group.,” *Lancet*, vol. 352, no. 9131, pp. 837–53, Sep. 1998.

[89] “Effect of intensive diabetes treatment on the development and progression of long-term complications in adolescents with insulin-dependent diabetes mellitus: Diabetes Control and Complications Trial,” *J Pediatr*, vol. 125, no. 2, pp. 177–188, Aug. 1994, doi: 10.1016/S0022-3476(94)70190-3.

[90] L. Z. Heng *et al.*, “Diabetic retinopathy: pathogenesis, clinical grading, management and future dev elopments,” *Diabetic Medicine*, vol. 30, no. 6, pp. 640–650, Jun. 2013, doi: 10.1111/dme.12089.

[91] P. H. Gallego, M. E. Craig, S. Hing, and K. C. Donaghue, “Role of blood pressure in development of early retinopathy in adolescents with type 1 diabetes: prospective cohort study,” *BMJ*, vol. 337, no. aug26 1, pp. a918–a918, Aug. 2008, doi: 10.1136/bmj.a918.

[92] R. Klein, M. D. Knudtson, K. E. Lee, R. Gangnon, and B. E. K. Klein, “The Wisconsin Epidemiologic Study of Diabetic Retinopathy XXIII: The Twenty-five-Year Incidence of Macular Edema in Persons with Type 1 Diabetes,” *Ophthalmology*, vol. 116, no. 3, pp. 497–503, Mar. 2009, doi: 10.1016/j.ophtha.2008.10.016.

[93] S. E. Mansour, D. J. Browning, K. Wong, H. W. Flynn Jr, and A. R. Bhavsar, “The Evolving Treatment of Diabetic Retinopathy,” *Clinical Ophthalmology*, vol. Volume 14, pp. 653–678, Mar. 2020, doi: 10.2147/OPTH.S236637.

[94] P. A. Campochiaro, “Reduction of Diabetic Macular Edema by Oral Administration of the Kinase Inhibitor PKC412,” *Investigative Opthalmology & Visual Science*, vol. 45, no. 3, p. 922, Mar. 2004, doi: 10.1167/iovs.03-0955.

[95]“Effect of Ruboxistaurin in Patients With Diabetic Macular Edema,” *Archives of Ophthalmology*, vol. 125, no. 3, p. 318, Mar. 2007, doi: 10.1001/archopht.125.3.318.

[96] L. A. Everett and Y. M. Paulus, “Laser Therapy in the Treatment of Diabetic Retinopathy and Diabetic Macular Edema,” *Curr Diab Rep*, vol. 21, no. 9, p. 35, Sep. 2021, doi: 10.1007/s11892-021-01403-6.

[97] A. Arrigo, E. Aragona, and F. Bandello, “VEGF-targeting drugs for the treatment of retinal neovascularization in diabetic retinopathy,” *Ann Med*, vol. 54, no. 1, pp. 1089–1111, Dec. 2022, doi: 10.1080/07853890.2022.2064541.

[98] H. El Rami, R. Barham, J. K. Sun, and P. S. Silva, “Evidence-Based Treatment of Diabetic Retinopathy,” *Semin Ophthalmol*, vol. 32, no. 1, pp. 67–74, Jan. 2017, doi: 10.1080/08820538.2016.1228397.

[99] P. Mitchell, G. Liew, B. Gopinath, and T. Y. Wong, “Age-related macular degeneration,” *The Lancet*, vol. 392, no. 10153. Lancet Publishing Group, pp. 1147–1159, Sep. 29, 2018. doi: 10.1016/S0140-6736(18)31550-2.

[100] R. Klein *et al.*, “Harmonizing the Classification of Age-related Macular Degeneration in the Three-Continent AMD Consortium,” *Ophthalmic Epidemiol*, vol. 21, no. 1, pp. 14–23, Feb. 2014, doi: 10.3109/09286586.2013.867512.

[101] M. V. Cicinelli *et al.*, “Optical coherence tomography angiography in dry age-related macular degeneration,” *Surv Ophthalmol*, vol. 63, no. 2, pp. 236–244, Mar. 2018, doi: 10.1016/j.survophthal.2017.06.005.

[102] W. Smith *et al.*, “Risk factors for age-related macular degeneration,” *Ophthalmology*, vol. 108, no. 4, pp. 697–704, Apr. 2001, doi: 10.1016/S0161-6420(00)00580-7.

[103] C. M. G. Cheung and T. Y. Wong, “Is age-related macular degeneration a manifestation of systemic disease? New prospects for early intervention and treatment,” *J Intern Med*, vol. 276, no. 2, pp. 140–153, Aug. 2014, doi: 10.1111/joim.12227.

[104] C. J. Thomas, R. G. Mirza, and M. K. Gill, “Age-Related Macular Degeneration,” *Medical Clinics of North America*, vol. 105, no. 3, pp. 473–491, May 2021, doi: 10.1016/j.mcna.2021.01.003.

[105] M. Homayouni, “Vascular endothelial growth factors and their inhibitors in ocular neovascular disorders.,” *J Ophthalmic Vis Res*, vol. 4, no. 2, pp. 105–14, Apr. 2009.

[106] A. C. Bird *et al.*, “An international classification and grading system for age-related maculopathy and age-related macular degeneration,” *Surv Ophthalmol*, vol. 39, no. 5, pp. 367–374, Mar. 1995, doi: 10.1016/S0039-6257(05)80092-X.

[107] “A Simplified Severity Scale for Age-Related Macular Degeneration,” *Archives of Ophthalmology*, vol. 123, no. 11, p. 1570, Nov. 2005, doi: 10.1001/archopht.123.11.1570.

[108] K. M. Gehrs, D. H. Anderson, L. V. Johnson, and G. S. Hageman, “Age- related macular degeneration—emerging pathogenetic and therapeutic concepts,” *Ann Med*, vol. 38, no. 7, pp. 450–471, Jan. 2006, doi: 10.1080/07853890600946724.

[109] J. E. Grunwald *et al.*, “Incidence and Growth of Geographic Atrophy during 5 Years of Comparison of Age-Related Macular Degeneration Treatments Trials,” *Ophthalmology*, vol. 124, no. 1, pp. 97–104, Jan. 2017, doi: 10.1016/j.ophtha.2016.09.012.

[110] M. Fleckenstein *et al.*, “The Progression of Geographic Atrophy Secondary to Age-Related Macular Degeneration,” *Ophthalmology*, vol. 125, no. 3, pp. 369–390, Mar. 2018, doi: 10.1016/j.ophtha.2017.08.038.

[111] R. Klein, B. E. K. Klein, S. C. Tomany, S. M. Meuer, and G.-H. Huang, “Ten-year incidence and progression of age-related maculopathy: The Beaver Dam eye study1 1The authors have no proprietary interest in the products or devices mentioned herein.,” *Ophthalmology*, vol. 109, no. 10, pp. 1767–1779, Oct. 2002, doi: 10.1016/S0161-6420(02)01146-6.

[112] S. Parmet, C. Lynm, and R. M. Glass, “Age-Related Macular Degeneration,” *JAMA*, vol. 295, no. 20, p. 2438, May 2006, doi: 10.1001/jama.295.20.2438.

[113] “A Randomized, Placebo-Controlled, Clinical Trial of High-Dose Supplementation With Vitamins C and E, Beta Carotene, and Zinc for Age-Related Macular Degeneration and Vision Loss,” *Archives of Ophthalmology*, vol. 119, no. 10, p. 1417, Oct. 2001, doi: 10.1001/archopht.119.10.1417.

[114] H. Zhou, H. Zhang, A. Yu, and J. Xie, “Association between sunlight exposure and risk of age-related macular degeneration: a meta-analysis,” *BMC Ophthalmol*, vol. 18, no. 1, p. 331, Dec. 2018, doi: 10.1186/s12886-018-1004-y.

[115] A. B. Enríquez *et al.*, “Early Experience With Brolucizumab Treatment of Neovascular Age-Related Macular Degeneration,” *JAMA Ophthalmol*, vol. 139, no. 4, p. 441, Apr. 2021, doi: 10.1001/jamaophthalmol.2020.7085.

[116] R. H. ElSheikh, M. Z. Chauhan, and A. B. Sallam, “Current and Novel Therapeutic Approaches for Treatment of Neovascular Age-Related Macular Degeneration,” *Biomolecules*, vol. 12, no. 11, p. 1629, Nov. 2022, doi: 10.3390/biom12111629.

[117] G. Virgili, R. Acosta, S. A. Bentley, G. Giacomelli, C. Allcock, and J. R. Evans, “Reading aids for adults with low vision,” *Cochrane Database of Systematic Reviews*, vol. 2018, no. 4, Apr. 2018, doi: 10.1002/14651858.CD003303.pub4.

[118] M. Ip and A. Hendrick, “Retinal vein occlusion review,” *Asia-Pacific Journal of Ophthalmology*, vol. 7, no. 1. Asia-Pacific Academy of Ophthalmology, pp. 40–45, Jan. 01, 2018. doi: 10.22608/APO.2017442.

[119] S. Rogers *et al.*, “The Prevalence of Retinal Vein Occlusion: Pooled Data from Population Studies from the United States, Europe, Asia, and Australia,” *Ophthalmology*, vol. 117, no. 2, 2010, doi: 10.1016/j.ophtha.2009.07.017.

[120] N. Cheung *et al.*, “Traditional and novel cardiovascular risk factors for retinal vein occlusion: The multiethnic study of atherosclerosis,” *Invest Ophthalmol Vis Sci*, vol. 49, no. 10, pp. 4297–4302, Oct. 2008, doi: 10.1167/iovs.08-1826.

[121] Y. C. Yen, S. F. Weng, H. A. Chen, and Y. S. Lin, “Risk of retinal vein occlusion in patients with systemic lupus erythematosus: A population-based cohort study,” *British Journal of Ophthalmology*, vol. 97, no. 9, pp. 1192–1196, Sep. 2013, doi: 10.1136/bjophthalmol-2013-303265.

[122] G. E. Lang and C. W. Spraul, “Risk factors for retinal vein occlusion,” *Tagliche Praxis*, vol. 43, no. 4. Hans Marseille Verlag GmbH, pp. 787–794, 2002. doi: 10.1016/s0161-6420(92)31940-2.

[123] Adil Jaulim, Badia Ahmed, Tina Khanam, and Irini P Chatziralli, “Branch retinal vein occlusion: epidemiology, pathogenesis, risk factors, clinical features, diagnosis, and complications. An update of the literature,” *Retina*, 2013, doi: 10.1097/IAE.0b013e3182870c15.

[124] N. L. B. Christoffersen and M. Larsen, “Pathophysiology and Hemodynamics of Branch Retinal Vein Occlusion,” 1999.

[125] S. S. Hayreh, P. A. Podhajsky, and M. B. Zimmerman, “Natural history of visual outcome in central retinal vein occlusion,” *Ophthalmology*, vol. 118, no. 1, pp. 119-133.e2, 2011, doi: 10.1016/j.ophtha.2010.04.019.

[126] M. K. Robinson and J. I. Halpern, “Retinal vein occlusion.,” *Am Fam Physician*, vol. 45, no. 6, pp. 2661–6, Jun. 1992.

[127] R. Lattanzio, A. Torres Gimeno, M. Battaglia Parodi, and F. Bandello, “Retinal vein occlusion: Current treatment,” *Ophthalmologica*, vol. 225, no. 3. pp. 135–143, Mar. 2011. doi: 10.1159/000314718.

[128] Wang, L et al.Trends in the application of deep learning networks in medical image analysis: Evolution between 2012 and 2020. Eur J Radiol. 146:110069 (2022).

[129] Abirami, M.S., Vennila, B., Suganthi, K., Sarthak, K., Anuja, V. Detection of Choroidal Neovascularization (CNV) in Retina OCT Images Using VGG16 and DenseNet CNN. Wireless Pers Commun. 127, 2569–2583 (2022).

[130] C Khan, Z. et al. (2021). Diabetic Retinopathy Detection Using VGG-NIN a Deep Learning Architecture. IEEE Access. 9, 61408-61416 (2021).

[131] Sashikanta, P., Sujit, K.D., Srikanta, P. A Novel Transfer Learning Technique for Detecting Breast Cancer Mammograms Using VGG16 Bottleneck Feature. ECS Trans. 107, 733-746 (2022).

[132] Anindya Apriliyanti, P. et al. UNet-VGG16 with transfer learning for MRI-based brain tumor segmentation. TELKOMNIKA. Vol 18, 3, 1310-1318 (2020).
[133] D. Albashish, R., Al-Sayyed, A., Abdullah, M.H.R., Nedaa, A.A. Deep CNN Model based on VGG16 for Breast Cancer Classification. International Conference on Information Technology (ICIT). 805-810 (2021).
[134] Jiang, Z.P., Yi-Yang, L., Zhen-En, S., Ko-Wei, H. 2021. An Improved VGG16 Model for Pneumonia Image Classification. Applied Sciences. 23: 11185 (2021).
[135] Kingma, D.P., Ba, J.. Adam: A Method for Stochastic Optimization. December 2014 (2014).
[136] Pedregosa, F. et al. Scikit-learn: Machine Learning in Python. J Mach Learn Res. 12(85):2825-2830 (2011).
[137] Spaide, R.F., Fujimoto, J.G., Waheed, N.K., Sadda, S.R., Staurenghi, G. Optical coherence tomography angiography. Prog Retin Eye Res. 64:1-55 (2018).
[138] Laíns, I. et al. Retinal applications of swept source optical coherence tomography (OCT) and optical coherence tomography angiography (OCTA). Prog Retin Eye Res. 84:100951 (2021).
[139] Schneider, E.W., Fowler, S.C. Optical coherence tomography angiography in the management of age-related macular degeneration. Curr Opin Ophthalmol. 29(3):217-225 (2018).
[140] Corvi, F., Cozzi, M., Invernizzi, A., Pace, L., Sadda, S.R., Staurenghi, G. Optical coherence tomography angiography for detection of macular neovascularization associated with atrophy in age-related macular degeneration. Graefe's Arch Clin Exp Ophthalmol. 259(2):291-299 (2021).
[141] Lindtjørn, B., Krohn, J., Forsaa, V.A. Optical coherence tomography features and risk of macular hole formation in the fellow eye. BMC Ophthalmol. 21:351 (2021).
[142] Ting, D.S.W. et al. Development and validation of a deep learning system for diabetic retinopathy and related eye diseases using retinal images from multiethnic populations with diabetes. JAMA - J Am Med Assoc. 318(22):2211-2223 (2017).
[143] Abbas, Q., Fondon, I., Sarmiento, A., Jiménez, S., Alemany, P. Automatic recognition of severity level for diagnosis of diabetic retinopathy using deep visual features. Med Biol Eng Comput. 55(11):1959-1974 (2017).
[144] Li, F., Chen, H., Liu, Z., Zhang, X., Wu, Z. Fully automated detection of retinal disorders by image-based deep learning. Graefe's Arch Clin Exp Ophthalmol. 257(3):495-505 (2019).
[145] Schlegl, T. et al. Fully Automated Detection and Quantification of Macular Fluid in OCT Using Deep Learning. Ophthalmology. 125(4):549-558 (2018).
[146] Lee, C.S., Tyring, A.J., Deruyter, N.P., Wu, Y., Rokem, A., Lee, A.Y. Deep-learning based, automated segmentation of macular edema in optical coherence tomography. Biomed Opt Express. 8(7):3440 (2017).
[147] Kermany, D.S. et al. Identifying Medical Diagnoses and Treatable Diseases by Image-Based Deep Learning. Cell. 172(5):1122-1131.e9 (2018).
[148] Abràmoff, M.D. et al. Improved automated detection of diabetic retinopathy on a publicly available dataset through integration of deep learning. Investig Ophthalmol Vis Sci. 57(13):5200-5206 (2016).
[149] Burlina, P., Freund, D.E., Joshi, N., Wolfson, Y., Bressler, N.M. Detection of age-related macular degeneration via deep learning. In: Proceedings - International Symposium on Biomedical Imaging. Vol 2016-June. Czech Republic; 184-188 (2016).

[150] Russakoff, D.B., Lamin, A., Oakley, J.D., Dubis, A.M., Sivaprasad, S. Deep learning for prediction of AMD progression: A pilot study. Investig Ophthalmol Vis Sci. 60(2):712-722 (2019).
[151] Thakoor, K.A. et al. A multimodal deep learning system to distinguish late stages of AMD and to compare expert vs. AI ocular biomarkers. Sci Rep. 12(1):2585 (2022).
[152] Saha, S. et al. Automated detection and classification of early AMD biomarkers using deep learning. Sci Rep. 9(1) (2019).
[153] Vyas, A., Raman, S., Surya, J., Sen, S., Raman, R. The Need for Artificial Intelligence Based Risk Factor Analysis for Age-Related Macular Degeneration: A Review. Diagnostics. 13(1) (2023).
[154] Samagaio, G., Estévez, A., Moura, J., Novo, J., Fernández, M.I., Ortega, M. Automatic macular edema identification and characterization using OCT images. Comput Methods Programs Biomed. 163:47-63 (2018).
[155] Saha, S., Nassisi, M., Wang, M. et al. Automated detection and classification of early AMD biomarkers using deep learning. Sci Rep 9, 10990 (2019).
[156] Thakoor, K.A., Yao, J., Bordbar, D. et al. A multimodal deep learning system to distinguish late stages of AMD and to compare expert vs. AI ocular biomarkers. Sci Rep 12, 2585 (2022).
[157] Yanagihara, R.T., Lee, C.S., Ting, D.S.W., Lee, A.Y. Methodological challenges of deep learning in optical coherence tomography for retinal diseases: A review. Transl Vis Sci Technol. 9(2) (2020).
[158] Son, J., Shin, J.Y., Kong, S.T. et al. An interpretable and interactive deep learning algorithm for a clinically applicable retinal fundus diagnosis system by modelling finding-disease relationship. Sci Rep 13, 5934 (2023).
[159] Lu, W., Tong, Y., Yu, Y., Xing, Y., Chen, C., Shen, Y. Deep learning-based automated classification of multi-categorical abnormalities from optical coherence tomography images. Transl Vis Sci Technol. 7(6) (2018).
[160] Rajagopalan, N., N V, Josephraj, A.N., E S. Diagnosis of retinal disorders from Optical Coherence Tomography images using CNN. PLoS One. 27;16(7):e0254180 (2021).
[161] Kurmann, T., Yu, S., Márquez-Neila, P. et al. Expert-level Automated Biomarker Identification in Optical Coherence Tomography Scans. Sci Rep 9, 13605 (2019).
[162] Lee, C.S., Baughman, D.M., Lee, A.Y. Deep Learning Is Effective for Classifying Normal versus Age-Related Macular Degeneration OCT Images. Ophthalmol Retin. 1(4):322-327 (2017).
[163] Choi, K.J. et al. Deep learning models for screening of high myopia using optical coherence tomography. Sci Rep. 11(1):21663 (2021).
[164] Kennedy, A.G. Imaging, Representation and Diagnostic Uncertainty. In: Lalumera, E., Fanti, S. Philosophy of Advanced Medical Imaging. Springer Briefs in Ethics. Springer, Cham. (2020).
[165] Aggarwal, R., Sounderajah, V., Martin. G., Ting, D.S.W., Karthikesalingam, A., King, D., Ashrafian, H., Darzi, A. Diagnostic accuracy of deep learning in medical imaging: a systematic review and meta-analysis. NPJ Digit Med. 4(1):65 (2021).
[166] Varoquaux, G., Cheplygina, V. Machine learning for medical imaging: methodological failures and recommendations for the future. NPJ Digit Med. 5(1):48 (2022).